# 16

# Examples of Organic Reactions on Zeolites: Methanol to Hydrocarbon Catalysis

**James F. Haw and David M. Marcus**
*University of Southern California, Los Angeles, California, U.S.A.*

## I. INTRODUCTION

Solid (heterogeneous) catalysts (1–4) are favored in industrial processes because they eliminate the need to separate the catalyst from the products. Heterogeneous catalysts can be solid acids, bases, supported metals, mixed metal oxides, or multifunctional materials. Commercial processes based on solid acids outnumber all others, and zeolites (and closely related materials) are usually the solid acids of choice. Many solvents and bulk chemicals are produced using zeolites as are important consumer goods such as gasoline. Although zeolites are not used to synthesize high polymers, they are essential for the production of the corresponding monomers. For example, *p*-xylene is obtained in high yield by toluene disproportionation or by the reaction of benzene and methanol in zeolite HZSM-5. Affordable *p*-xylene allows production of *p*-terpthalic acid and hence polyethylenetelephthalate (PET) polymer (plastic soda bottles). Methanol conversion on modified HZSM-5 or various silicoaluminophosphate catalysts produces propene and ethylene in high yields, and the production of polyolefins by way of methanol will soon be common. Zeolite catalysts such as HBEA (beta) are used to convert benzene and propene to cumene, which in turn is converted to acetone and phenol by selective oxidation (cumene hydroperoxide chemistry). Other heteroatom-containing products are produced directly by reactions in zeolites. For example, pyridine and picolines are produced on HZSM-5 from a mixture of ammonia and aldehydes or ketones, especially formaldehyde, acetaldehyde, and acetone.

In-depth coverage of all organic reactions on zeolites would require a dedicated volume. We have chosen instead to focus on the process we know best, and that is methanol conversion to hydrocarbons (5–10). Through this process we will at least briefly touch on many important zeolite-catalyzed reactions, such as ether synthesis, cracking, isomerization, and so forth. This approach will also permit an in-depth treatment of one important reaction mechanism. We will see that many mechanisms have been proposed for this chemistry, which in turn have motivated many experimental and theoretical studies. This is not unique to methanol conversion; there is no consensus on the mechanisms of most organic reactions in zeolites, even seemingly simple ones such as butane isomerization to isobutane. This lack of insight into mechanism does not prevent

the chemical industry from supplying many of our material needs, but it does vex academic scientists interested in surface chemistry and catalysis. Progress in understanding the mechanisms of zeolite-catalyzed reactions may or may not contribute to the rational design of improved catalysts, but it would certainly raise the stature of the field in the eyes of chemists who work on more easily tractable mechanistic problems in the gas phase or solution.

## II. MATERIALS AND MECHANISMS

The other contributions to this book have covered zeolite structure to a much greater degree than is appropriate for a chapter on organic reactions. The most important properties of a zeolite as a catalyst for organic reactions include framework topology, acid strength, acid site density, and crystallite size. The latter sometimes is important for controlling secondary reactions as small crystallites provide for rapid mass transfer. Here we briefly review only those materials that are most commonly used in fundamental studies of methanol conversion chemistry.

### A. Aluminosilicate Zeolites

Figure 1 compares views down the straight channels of the aluminosilicate zeolites HZSM-5 (MFI) and HBEA. Both catalysts have intersecting channel systems; HZSM-5 is a medium-pore zeolite with 10-rings in both channels, while the large-pore HBEA has 12-rings. HZSM-5 was used as a commercial methanol to gasoline catalyst, and newer catalysts obtained by modification of this zeolite may be useful for the production of other hydrocarbon products. HBEA is sometimes used for mechanistic studies in methanol conversion catalysis because its larger channels permit the entrance and exit of larger molecules such as hexamethylbenzene.

The Si/Al ratio, and hence acid site density, is widely variable in both HZSM-5 and HBEA. At the lower end, solid acids with Si/Al in the range of 12–20 can be prepared, but larger values, up to several hundred, are more common. In the past it was commonly believed that the acid strength of HZSM-5 increases as the acid sites become increasingly isolated. For example, HZSM-5 with Si/Al = 300 was believed to be a much stronger acid than the same framework with Si/Al = 100. This almost certainly overstates the effect of Si/Al ratio on acid strength. Higher acid site densities do tend to promote secondary reactions. Zeolites with very high acid site concentrations (e.g., Si/Al of 20 or lower) have "paired" sites that may have special activity for some reactions.

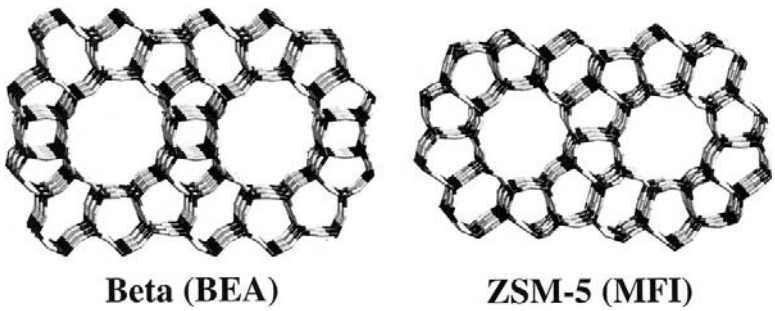


**Fig. 1** Structures of the aluminosilicate zeolites HZSM-5 and HBEA. Views down the straight channels are shown.

## B. Silicoaluminophosphates

Although the term zeolite is sometimes restricted to aluminosilicates, "zeotypes" with other framework compositions are so commonly studied by zeolite chemists that a more inclusive definition is used here. Figure 2 shows the very similar topologies of HSAPO-34 (CHA) and HSAPO-18 (AEI). Both are composed of nanometer-sized cages interconnected by 8-rings; thus, they are small-pore materials. Aromatics, even benzene, cannot enter or leave these cages, nor can branched alkanes or olefins. Beyond topology, these silicoaluminophosphate (SAPO) catalysts also differ from HZSM-5 in acid strength. For example, ethylene can be flowed over a freshly activated HSAPO-34 catalyst bed at 375°C without the immediate appearance of other hydrocarbons in the product stream, but ethylene is very reactive on HZSM-5 under identical conditions.

In principle, the substitution of silicon for phosphorus into an aluminosilicate lattice produces a framework acid site. At lower silicon contents this is generally true; it is fairly easy to synthesize HSAPO-34 with one template molecule in each cage and one acid site per cage in the calcined material. At higher Si concentrations, silicous islands begin to form, reducing the number of acid sites below one per silicon.

## C. Methanol to Hydrocarbon Processes

Methanol is made from methane through mature catalytic processes. First natural gas is steamed over a supported Ni catalyst to form syn gas, a mixture of CO, $CO_2$, and $H_2$. This, in turn, is converted to methanol with extraordinary selectivity using $Cu/ZnO/Al_2O_3$ catalyst at about 50 atm and 250°C. Methanol is an inexpensive intermediate; thus, processes for converting it to transportation fuels or consumer goods allow us to make better use of methane without waiting for direct methane conversion, which could be a long wait.

Global methanol capacity was expanded in the 1990s to meet the anticipated demand for the gasoline additive methyltertbutylether (MTBE). Reformulated gasolines containing 10–20% MTBE burn more cleanly than conventional oxygen-free fuels. Unfortunately, MTBE has a foul taste that can be sensed in water containing a trace. Underground gasoline storage tanks leak, and MTBE rapidly moves through the water table, entering potable water supplies through wells. A well-thought-out strategy for reducing one environmental problem gave rise to another, and MTBE is being phased out, perhaps to be replaced by

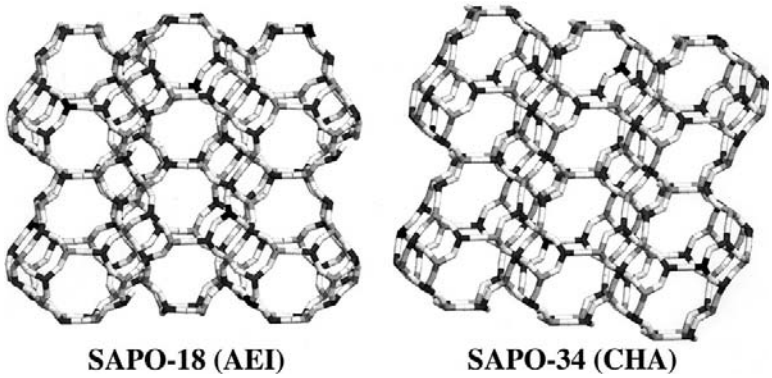


**Fig. 2** Structures of the silicoaluminophosphates HSAPO-34 and HSAPO-18. Both materials have nanometer-sized cages interconnected by much smaller windows.

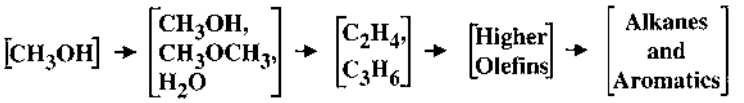


**Scheme 1** Methanol to hydrocarbons.

a more palatable oxygenate distilled from corn mash. Meanwhile the petrochemical industry is awash in methanol.

### 1. Methanol to Gasoline

Scheme 1 depicts in a simple way the chemistry in methanol conversion catalysis. Methanol rapidly equilibrates to a mixture of starting material and its condensation products, dimethyl ether (DME) and water. This process is frequently taken to be a pre-equilibrium. Industrially, it may even occur in a separate reactor to better control the temperature of the second reactor in which hydrocarbon synthesis occurs. The primary hydrocarbon products are light olefins, a mixture of ethylene and propene with smaller amounts of $C_4$ olefins. On solid acids of sufficient strength, light olefins readily oligomerize to higher olefins that may in turn crack to an equilibrium distribution. Also, in the presence of excess methanol, the primary olefinic products may homologize to the next higher olefins; for example, propene may react with methanol to make butene. Finally, on stronger solid acids, complex reactions involving hydride transfer can convert olefins to a mixture of branched alkanes and methylbenzenes. With the correct process conditions this mixture can be very much like the kinds of gasolines favored in the 1980s. Indeed, the methanol to gasoline (MTG) process using zeolite HZSM-5 was commercialized in New Zealand in the 1980s, and for a time it produced about 30% of that country's needs, although a heavy government subsidy was required. Environmental considerations are reducing the desirability of aromatics in gasoline, and the return of MTG would require a grave petroleum shortage.

### 2. Methanol to Olefin

If refineries are already producing too much aromatics, they are not producing enough ethylene and propene. Every human on earth consumes, on average, several pounds of polyethylene per year. Refineries produce light olefins as byproducts of gasoline, either directly or by steam-cracking light alkanes. Many refineries have associated polyolefin plants. But the demand for polyolefins is growing rapidly, and refineries will not be able to meet demand. Referring again to Scheme 1, if the conversion of methanol to hydrocarbons could be stopped after formation of light olefins, methane could be the ultimate feedstock for polyolefins. Plans for integrated chemical plants converting natural gas to polymers have already been announced, and methanol to olefin (MTO) catalysis is central to their operation, all other technologies being mature.

Earlier we introduced several methanol conversion catalysts; Fig. 3 reports gas chromatography (GC) traces analyzing the products exiting identical benchtop flow reactors converting methanol under identical conditions on catalyst beds of either the aluminosilicate HZSM-5 or the silicoaluminophosphate HSAPO-34. Also, Fig. 3 illustrates more broadly the considerable differences in selectivity resulting from differences in topology and acidity between two microporous solid acids. Such differences are pervasive in zeolite catalysis.

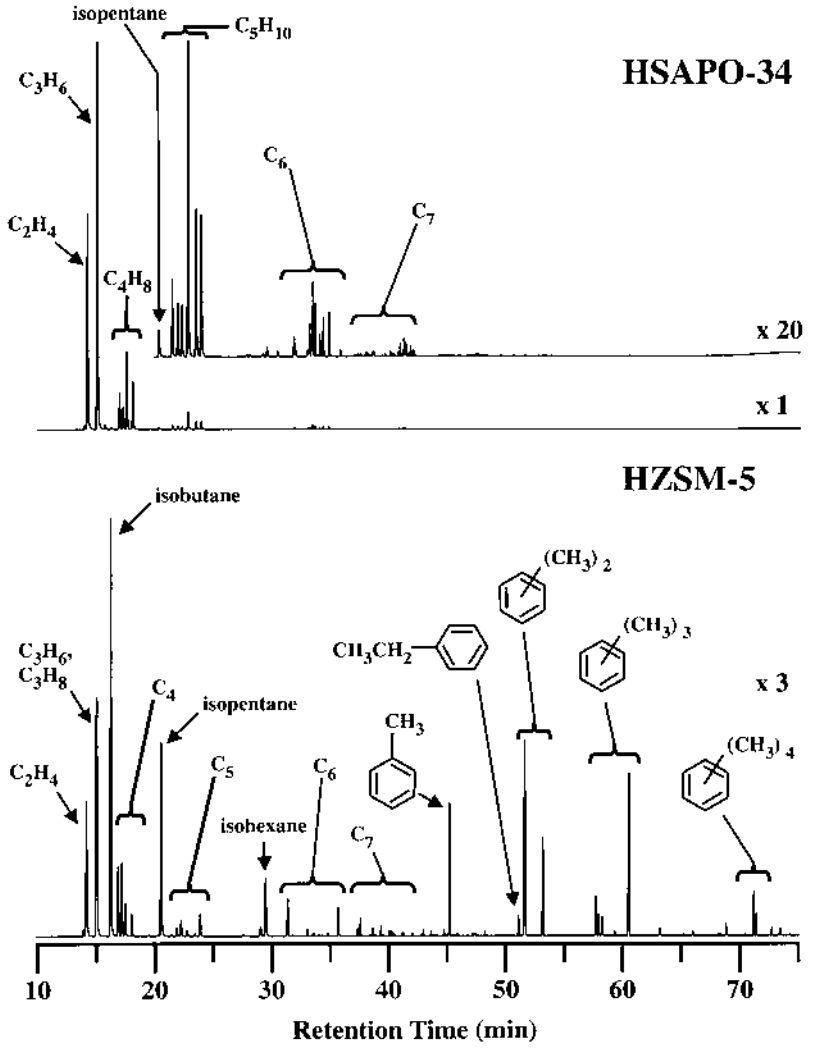


**Fig. 3** GC (FID detection) traces comparing the volatile products formed during methanol conversion on HSAPO-34 and HZSM-5. Experimental conditions were otherwise identical, 375°C, and methanol space velocity of 8 $h^{-1}$. On HSAPO-34 the products are ethylene, propene, small amounts of butenes, and traces of other compounds including light alkanes. This is characteristic of MTO catalysis. On HZSM-5 secondary reactions catalyzed by stronger acid sites lead to greater yields of alkanes and aromatics (MTG catalysis). The latter are able to exit the medium pore zeolite catalyst.

In evaluating results such as Fig. 3 it is important to know some of the exact experimental details—not just temperature and catalyst composition, but also the manner and history of reagent introduction. It is sometimes useful to study the transient response of a catalyst after one or more pulses of reagent. Alternatively (as in Fig. 3), the catalyst is studied under steady-state conditions using continuous introduction of reagent at some specified "space velocity." The latter is conveniently defined as the (mass of feed)/(mass of catalyst × unit time). In laboratory experiments, a motor-driven syringe pump is used to

deliver reagent at a controlled rate. As a catalyst bed ages its activity and selectivity change, and the former trends toward zero as the catalyst deactivates. Thus, steady-state behavior is only approximately so; in the case of Fig. 3 the two catalysts were compared at the same times on stream, both well before activity began to fail.

### D. Mechanisms Proposed for MTG/MTO Chemistry

A recent review recognized at least 20 mechanisms proposed for methanol to hydrocarbon catalysis (9). These are usually identified by the key intermediate, and they typically lead to ethylene or a ready precursor of ethylene. Several recent theoretical studies have used computational chemistry to identify transition states connecting reactants and initial products without the involvement of distinctive intermediates (11,12). Including these there are probably many more than 20 distinct mechanisms in the literature. In the past several years a great deal of evidence has emerged in support of one or more pathways based on a pool of hydrocarbon intermediates in the catalyst (13–24). Present work (discussed later) is directed to the detailed structure and function of the hydrocarbon pool, and increasingly detailed (hence testable) proposals are emerging. First we review some of the classical mechanisms of methanol conversion catalysis.

#### 1. Several Distinct Oxonium Mechanisms

An oxonium cation is characterized by three-coordinate oxygen. Nuclear magnetic resonance (NMR) studies have shown that the trimethyloxonium cation can form by disproportionation of dimethyl ether on zeolite HZSM-5 (25,26). A second type of methoxonium species results from the condensation of a zeolite acid site with methanol. In this case it is an oxygen in the framework that is formally charged; of course, it is this same oxygen that is bound to a silicon, an aluminum, and a proton to form the underivatized acid site. Again, NMR studies have provided much evidence for "framework-bound methoxy" species in zeolites (27,28). These are most easily formed and observed by reacting a cation-exchanged basic zeolite such as CsY with methyl iodide.

Scheme 2 combines two distinct proposals (29,30) for the formation of the "first" C-C bond by way of trimethyloxonium ion. Both require deprotonation of the oxonium cation to an oxonium-ylide. They differ only in whether a subsequent methylation step is intramolecular (Stevens rearrangement) or intermolecular. A major problem is identifying a basic site strong enough to deprotonate the oxonium cation. In either case, ethylene elimination is assumed to occur rapidly. The mechanism in Scheme 3 also involves an oxonium-ylide, this time on the zeolite framework (31).

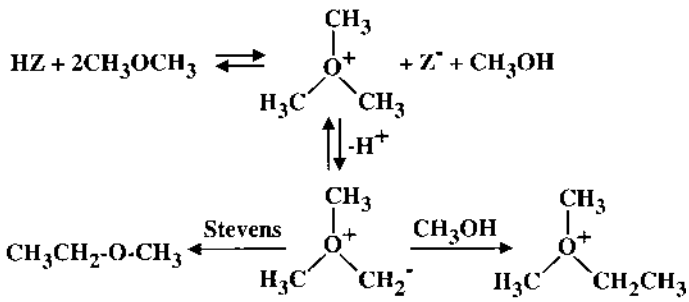


**Scheme 2** Two oxonium ylide mechanisms.

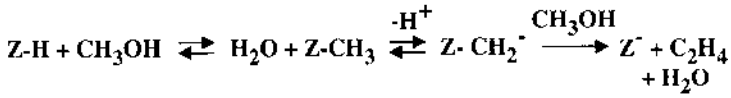

**Scheme 3** Framework oxonium ylide mechanism.

### 2. Carbocation Mechanisms

Scheme 4 shows one (32) of several similar proposals in which the equivalent of $CH_3^+$ (a carbenium ion) is transferred to a DME molecule to form a five-coordinate carbonium ion that affords ethylmethyl ether by deprotonation. Schemes such as this presumably require that the zeolite catalyst have exceptionally strong (superacidic) acid sites.

### 3. Carbene Mechanisms

Scheme 5 (33) and Scheme 6 (34) depict two literature mechanisms for the generation of highly reactive carbene ($CH_2$) intermediates in zeolites under methanol conversion conditions. Scheme 5 suggests how two proximal acid sites (one in conjugate base form) could work synergistically to dehydrate methanol to $CH_2$. Scheme 6 describes the formation of a framework methoxonium species (imagined as a $CH_3^+$, $Z^-$ ion pair) that eliminates carbene. This intermediate is so reactive that C-C bonds could form through any of several routes.

### 4. Radical Mechanisms

One (35) of several (35,36) radical chain reaction proposals is depicted in Scheme 7. Small electron spin resonance (ESR) signals can be detected on many zeolites under a variety of reaction conditions; otherwise spectroscopic evidence for radical mechanisms is weak.

### 5. Introduction to the Hydrocarbon Pool Mechanism

In the early 1980s Mole and coworkers observed that methanol conversion on HZSM-5 was accelerated by the "cocatalytic" effect of added toluene (37,38). They speculated that this effect resulted from alkylation of the side chains on aromatic rings leading to olefin elimination (Scheme 8).

In the 1990s Kolboe et al. carried out very important experiments on HSAPO-34 and other methanol catalysts in which they cofed olefin precursers, such as ethanol, with isotopically labeled methanol in order to study the isotopic composition of the reaction products in relation to time on stream (15–17). The distribution of isotopic labels was inconsistent with a direct reaction mechanism. Experiments such as this led Kolboe to propose that the first olefins in methanol conversion form on a "hydrocarbon pool," a collection of organic species in the catalyst. The structure of this pool was originally loosely specified. Scheme 9 (16) suggests that it may be some sort of alkane, but the possibility that it was a carbenium ion was also allowed for. A key feature of Scheme 9 is

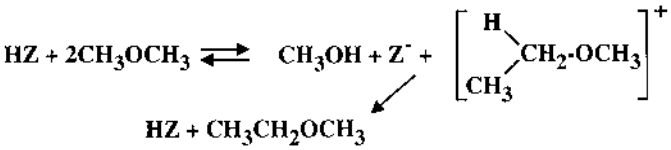

**Scheme 4** One of several carbocation mechanisms.

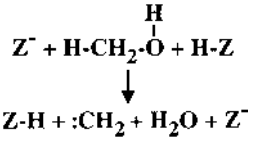

**Scheme 5** A carbene mechanism based on two zeolite acid sites.

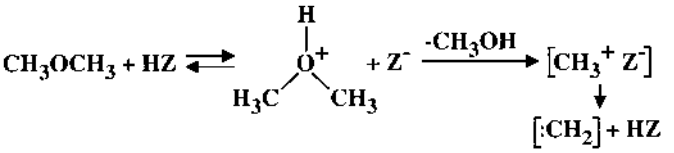

**Scheme 6** A mechanism in which a framework methoxonium forms a carbene.

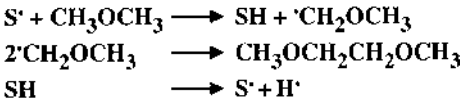

**Scheme 7** One of several free radical mechanisms. S• is an unspecified surface radical site.

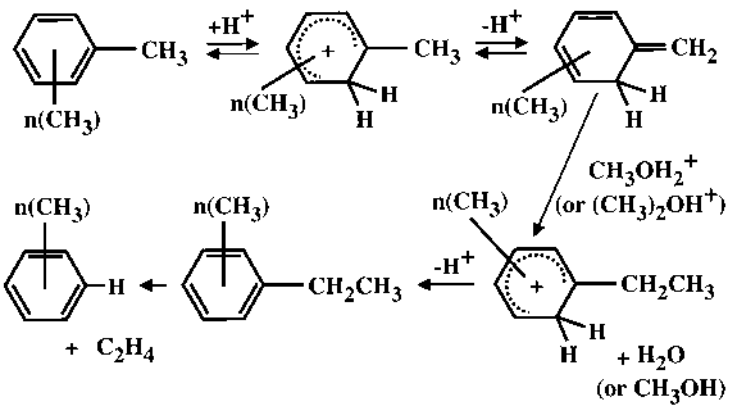

**Scheme 8** Mole's mechanism to explain the "cocatalytic" effect of toluene. This is the first detailed proposal for what is now called the hydrocarbon pool.

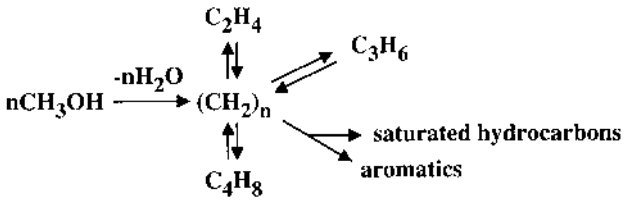


**Scheme 9** Kolboe's schematic hydrocarbon pool mechanism.

parallel synthesis of olefins; for example, the pool could eliminate ethylene, propene, or a $C_4$ olefin, forming each of these as the first volatile products with C-C bonds. Other mechanisms predict the formation of a single olefin (almost always ethylene) that is subsequently methylated to form larger olefins.

A number of studies have recently provided very strong support for hydrocarbon pool routes in MTO catalysis. Some of these are summarized later in the chapter.

## III. EXPERIMENTAL METHODS FOR MECHANISM STUDIES

### A. Benchtop Reactor Systems

Figure 4 depicts schematically a simple benchtop flow reactor that could be used to study organic reactions on zeolites and similar catalysts. The catalyst bed in such studies is usually a few hundred milligrams and rarely larger than a few grams. It is usually activated in place by heating to some temperature at or above the use temperature in an inert gas stream, frequently He. This gas is delivered at a specified flow rate using a mass flow controller. The reactor shown uses a valve to deliver a single pulse of liquid reactant. Motor-driven syringe pumps are used to study catalysts under steady-state conditions as well as deactivation over longer times on stream. The reactor (stainless steel or quartz) is regulated at the desired temperature. One or more gas samples are collected at various times and stored for GC or GC–mass spectrometry (MS) analysis. If the products have

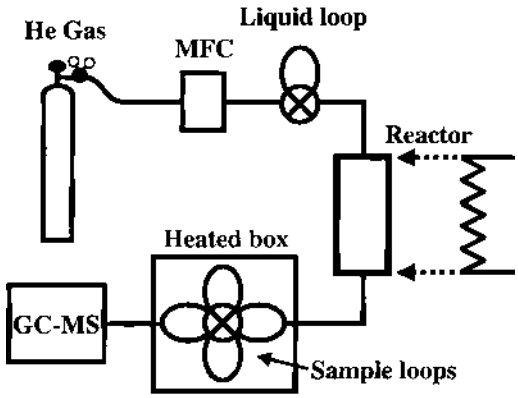


**Fig. 4** Schematic diagram of a bench-top flow reactor used for laboratory investigations of zeolite catalysis. MFC denotes mass flow controller, and GC-MS a gas chromatograph with mass spectrometric detection. The design shown delivers a pulse of liquid reactant using an automatic valve and collects multiple product gas samples (as a function of reaction time) for subsequent analysis.

low vapor pressures at room temperature, the sampling valve must be housed in a heated box and transfer lines may need to be heated as well. The two chromatograms in Fig. 3 were measured by capturing gas samples from catalyst beds operated under steady-state conditions. These samples were immediately injected into a gas chromatograph with flame ionization detection. GC-MS detectors generate similar chromatograms by summing the total ion intensities in each spectrum and plotting this against time. GC or GC-MS analysis is used in a great majority of all benchtop catalytic studies.

A great value of GC-MS analysis in catalysis involves the use of isotopic labels to probe reaction mechanisms. Figure 5 reports an example of this based on the fate of deuterium labels. Methylbenzenes are important components of the hydrocarbon pool in methanol to hydrocarbon chemistry on various catalysts. One characteristic reaction of methylbenzenes on acidic zeolites is disproportionation. For example, toluene dispropor-

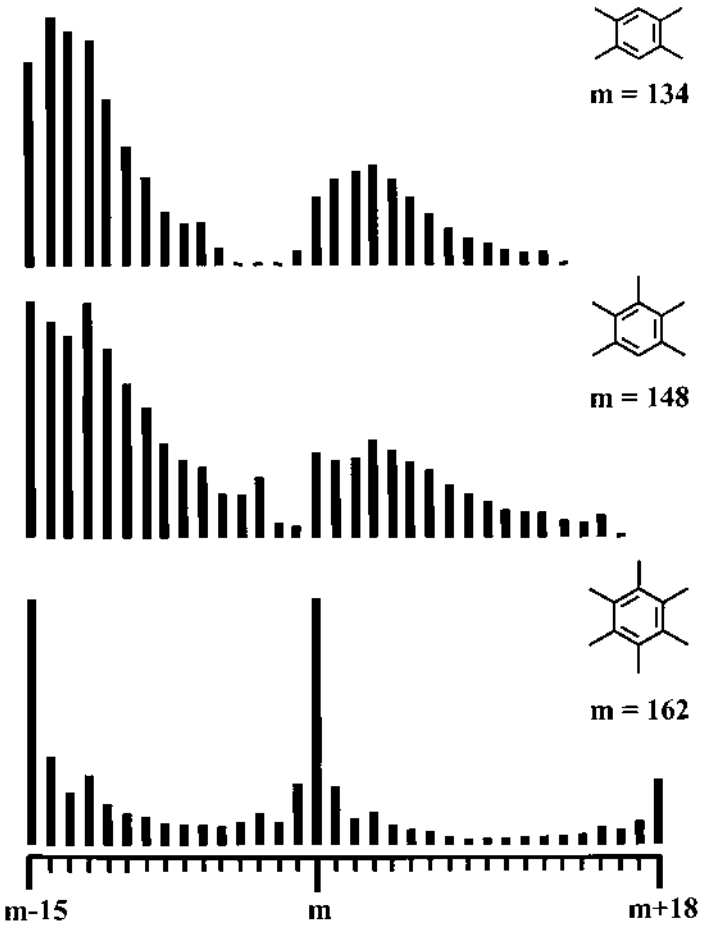


**Fig. 5** Bar graphs showing ion mass distributions in the vicinity of the molecular ions from GC-MS analyses of the volatile products exiting a catalytic reactor (300 mg zeolite HBEA, $SiO_2/Al_2O_3 = 75$, 450°C) 1.5 s following pulsed introduction of 0.62 mmol of HMB and 0.62 mmol HMB-$d_{18}$. The reactions leading to durene and pentamethylbenzene included extensive H/D exchange that occurred in steps of one.

tionates to a mixture that contains xylenes and benzenes (39). Hexamethylbenzene (HMB) also apparently disproportionates through a process described below; and when HMB is pulsed onto a zeolite HBEA catalyst bed at 450°C, the products exiting the reactor include pentamethylbenzene and isomers of tetramethylbenzene. For the experiment in Fig. 5, the HMB pulsed onto the catalyst was an equal mixture of normal HMB and HMB-$d_{18}$. Methyl exchange alone, without the making and breaking of C-H and C-D bonds, should result in products with masses grouped in units of three. For example, a simple exchange of methyl groups between HMB and HMB-$d_{18}$ would produce HMB molecules that are deuterated in multiples of three, e.g., HMB-$d_3$ and HMB-$d_6$, but not HMB-$d_1$ or HMB-$d_5$, etc. Figure 5 shows that HMB with all possible numbers of deuterium was obtained, and this is even more evident for pentamethyl- and tetramethylbenzenes. Thus, in addition to methyl exchange there is also a second exchange process that breaks C-H bonds and permits one-by-one deuterium exchange. This mechanism is discussed later in the contribution.

## B. In Situ Methods

Much of what we know about organic reactions in solution has come from spectroscopic studies. For example, a reaction might be carried inside of an NMR tube and spectra taken over the course of time will reveal kinetics and possibly intermediates. If a stable isotope label is selectively incorporated in one of the starting materials, the fate of that label, revealed by NMR, will frequently be instructive as to mechanism. In order to understand the mechanism of a zeolite-catalyzed reaction we would (ideally) like to be able to look inside of a catalytic reactor and observe the structure and energy of every intermediate and transition state along the reaction pathway. Of course, we cannot realize this entirely even in solution, but for zeolite catalysis the challenges are even greater. A typical industrial process using zeolites will be carried out at temperatures from 300°C to 500°C, and reaction times of 0.1 s to 10 s. Even thin wafers of zeolites absorb strongly over much of the electromagnetic spectrum. These conditions make fundamental mechanistic studies much more challenging than corresponding studies in solution, at lower temperatures and longer reaction times.

A variety of spectroscopic methods have been applied to understand reactions on zeolites. Such investigations are commonly called in situ (in its own place) studies because the goal is to understand the reaction as it occurs on the real catalyst under actual industrial conditions. Not surprisingly, essentially all in situ studies involve compromises between conditions that favor laboratory experiment and those that simulate industrial practice. There are a number of in situ methods, and many of these are reviewed in a recent book (40). Here for brevity we will consider only three: NMR, vibrational spectroscopy (IR and Raman), and theoretical modeling. The last is not strictly an experimental method, but the way in which a computational chemist approaches the modeling of a chemical reaction is in many ways similar to that in which a spectroscopist approaches the same problem. It is sometimes said that the experimental tool of a computational chemist is the supercomputer.

### 1. Nuclear Magnetic Resonance

There are a number of ways to use NMR to study organic reactions in zeolites in situ, each with their own strengths and limitations (41,42). These have been reviewed in greater detail recently (43); all of the applications reported here make use of the thermal quench method (44). A quench reactor is very much like the benchtop flow reactor diagrammed in Fig. 4 but with the addition of valves and plumbing that permit the catalyst bed to be cooled to

room temperature in a fraction of a second. The organic components in the quenched catalyst bed are frequently similar to those in the catalyst immediately prior to the quench, and NMR spectra measured on quenched catalysts can be used to make inferences about the organic composition of the catalyst bed under reaction conditions.

Zeolite catalysts are solids, and most molecules adsorbed in zeolites have the restricted mobility of solids. Thus, NMR experiments on organic matter in catalysts require many of the techniques of solid-state NMR, especially magic angle sample spinning. Proton spectra of complex solid materials are sometimes not chemically useful, and most in situ work is performed with $^{13}C$ NMR. Although only 1.1% of naturally occurring carbon is $^{13}C$, many simple organic compounds are available with high levels of $^{13}C$ enrichment.

Figure 6 shows $^{13}C$ solid-state NMR spectra of five HZSM-5 catalyst beds that each received a pulse of ethylene-$^{13}C_2$ and then reacted at 350°C at various times before

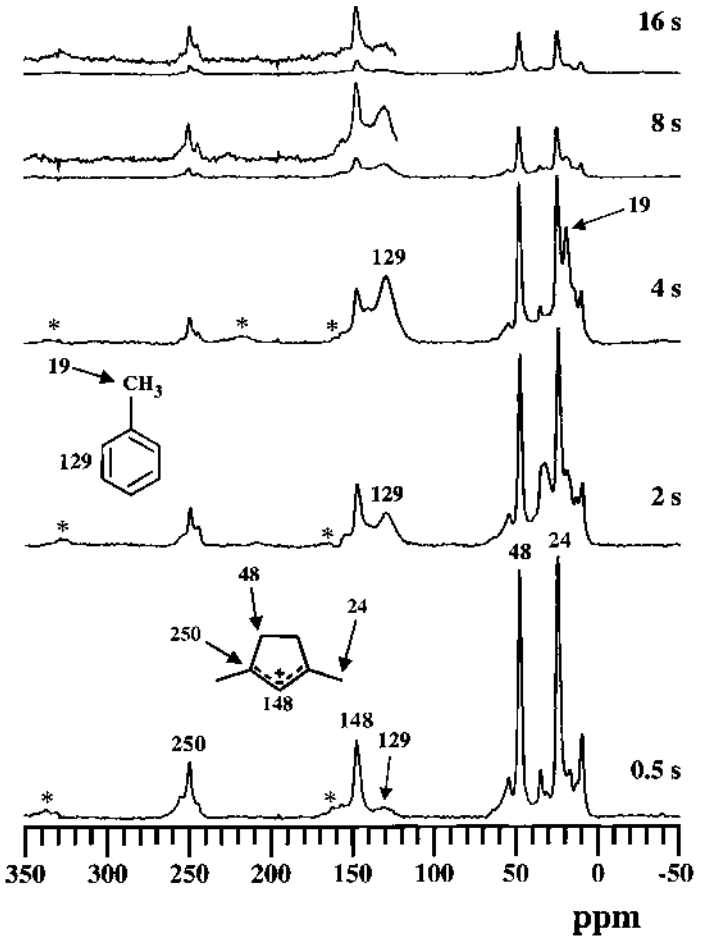


**Fig. 6** $^{13}C$ CP/MAS NMR spectra of the reaction products of ethylene-$^{13}C_2$ retained on zeolite HZSM-5 following various times at 350°C in a pulse-quench reactor. Signals from cyclopentenyl cations (250, 148, 48, and 24) and toluene (129 and 19) are indicated in the spectra. All spectra were measured at 25°C. The asterisks denote spinning sidebands.

thermal quenching (20). At the shortest time studied (0.5 s), the $^{13}C$ NMR spectrum shows that most of the organic matter entrained in the catalyst bed is accounted for by the 1,3-dimethylcyclopentenylcarbenium ion. After 2–4 s much of this cation is converted to toluene, which can readily escape from the medium-pore HZSM-5 catalyst. Most of the organic matter has left the catalyst bed after 8–16 s.

The stoichiometry of the reactions identified in Fig. 6 merits discussion. Ethylene (one of the primary products of methanol conversion catalysis) oligomerizes, cyclizes, and dehydrogenates to form the $C_7H_{11}^+$ cation, which is charge balanced by the conjugate base of the zeolite acid site, $Z^-$. Simply put, 3 1/2 ethylene molecules of stoichiometry $C_7H_{14}$ (and the proton of one acid site) must lose two equivalents of $H_2$ to form $C_7H_{11}^+$. Toluene is $C_7H_8$; one proton is transferred back to the zeolite, but a third equivalent of $H_2$ must be lost from the intermediate cyclopententyl cation in forming the aromatic product.

While molecular hydrogen is sometimes evolved from organic material on acidic zeolites, a more common way to lose hydrogen is through disproportionation reactions. MTG catalysis produces little or no olefins; instead the products are alkanes and aromatics. An olefin has one degree of unsaturation and a methylbenzene four, but an open-chain (as opposed to cyclic) alkane has none. Thus, stoichiometry suggests that we should see up to 3 moles of alkane for every mole of aromatic produced in methanol conversion catalysis. Conversely, if we are carrying out MTO catalysis using HSAPO-34 (a small-pore zeolite from which aromatics cannot escape) and we see some propane and *n*-butane in the product stream, we can infer the formation of aromatics in the cages of the catalyst.

## 2. Infrared and Raman Spectroscopy

Fourier Transform Infrared (FTIR) spectroscopy is frequently used to study zeolites, with or without organic adsorbates, and it can also be used to study reactions in situ under conditions that more closely approach industrial practice than for typical NMR experiments. This field has recently been reviewed by Howe (45). Usually this is done using thin pressed wafers of zeolite placed in the optical path and in contact with a flowing gas stream. Alternatively, the method of diffuse reflectance can be applied to zeolite powder placed in a heated ceramic cup with a gas stream passed through the reflectance cell. In either case the usable spectral window is restricted to frequencies above approximately 1100 $cm^{-1}$ due to the strong absorbance of zeolite framework modes at lower wavenumbers.

Much recent progress has been made in the application of Raman spectroscopy to zeolite catalysis, and this area has recently been reviewed (46). Many Raman measurements must deal with interference from sample fluorescence, but this can be largely overcome using UV-Raman equipment. A considerable amount of sample heating occurs with a UV laser; Stair has overcome this problem using an in situ cell that circulates zeolite catalyst as in a fluidized reactor. In situ Raman measurements have confirmed the formation of cyclopentenylcarbenium ions on zeolite HZSM-5 during methanol conversion catalysis.

## 3. Theoretical Modeling

Theoretical methods are widely applied to the study of zeolites and the structure, energetics, spectroscopic properties, diffusion, and reactions of organic species in zeolites. Commercial software packages are available for visualizing the structure of zeolites with or without organic adsorbates. These programs are useful in their own right and some

can also serve as interfaces for computational chemistry programs, such as Gaussian (47), that apply sophisticated electronic structural methods to parts of the zeolite-adsorbate structure.

Considering the rate of growth in computer power and progress in the development of theoretical methods that lend themselves to more efficient computations, we are perhaps a decade away from being able to compute many properties of zeolites and their interactions with adsorbates with accuracy comparable to that of experiment. A few years down the road it may be possible to model some of the simpler reactions on zeolite catalyst beds using rigorous theoretical methods to predict reaction pathways and the rates of various steps. Even today, in special circumstances with high symmetry, it is possible to use fully periodic calculations to calculate some properties using a structural model without boundaries. However, more typically it is necessary to make sometimes severe approximations to the zeolite structure in order to have a small enough number of electrons for the application of a reliable electronic structural theory.

The two structures in Fig. 7 are a case in point (20). Shown are cluster models of the acid site in zeolite HZSM-5. This is approximated using one aluminum T site, and seven silicon T sites, which are of course connected by bridging oxygen atoms. The cluster is terminated by capping the outermost silicons with hydrogens so that there are no dangling valences. These outermost silicons are also held fixed at their crystallographic locations during subsequent structural optimization steps, ensuring that the final structures are relevant to the structure of zeolites. The acid site corresponds to the proton on the oxygen-bridging Al and the central Si.

Each zeolite cluster in the figure has associated with it a derivative of 1,3-dimethylcyclopentadiene. In the case of 7a, the proton has transferred from the zeolite to the diene, protonating it to form the 1,3-dimethylcyclopentadienylcarbenium ion, the species observed experimentally in Fig. 6. Note that one of the hydrogens on the carbenium ion is directed toward the zeolite and forms a hydrogen bond with the zeolite anion site $Z^-$. In Fig. 7b this proton transfer has not occurred, and the structure shown is a $\pi$ complex of the neutral diene with the zeolite acid site HZ. The two structures in Fig. 7 were obtained through a structural optimization process in which small variations in atomic coordinates were made in a systematic manner, and the energy of the structure was calculated at each step (vide infra). Each optimization was complete when it converged to a local minimum in the potential energy surface for the structure. It is not uncommon to find two or more minima corresponding to different stable structures; in this case the two very similar structures shown differ primarily in the extent of proton transfer from the zeolite to the organic adsorbate.

The theoretical calculations in Fig. 7 revealed that the two structures (stable points on the potential energy surface) differ in energy by a very small amount, 2.2 kcal/mol, with the zwitterionic state (a) being slightly more stable than the $\pi$ complex (b). The significance of this finding is that proton transfer between the zeolite and the carbenium ion involves little energy penalty, and neutral and cationic organic species of the type shown in Fig. 7 are plausibly in equilibrium on the zeolite. We will see that similar equilibria for cations and neutral olefins on zeolites is an important characteristic of recently proposed hydrocarbon pool mechanisms for methanol conversion catalysis.

Computational chemistry methods use basis sets to approximate atomic orbitals and electronic structural theories to calculate observable properties such as energy or spectroscopic properties. The accuracy of a calculation depends on several factors: the structural model (e.g., cluster size), the electronic structural theory, and the basis sets used. Ideally, the computed results will converge toward a limiting value as the size of the basis sets

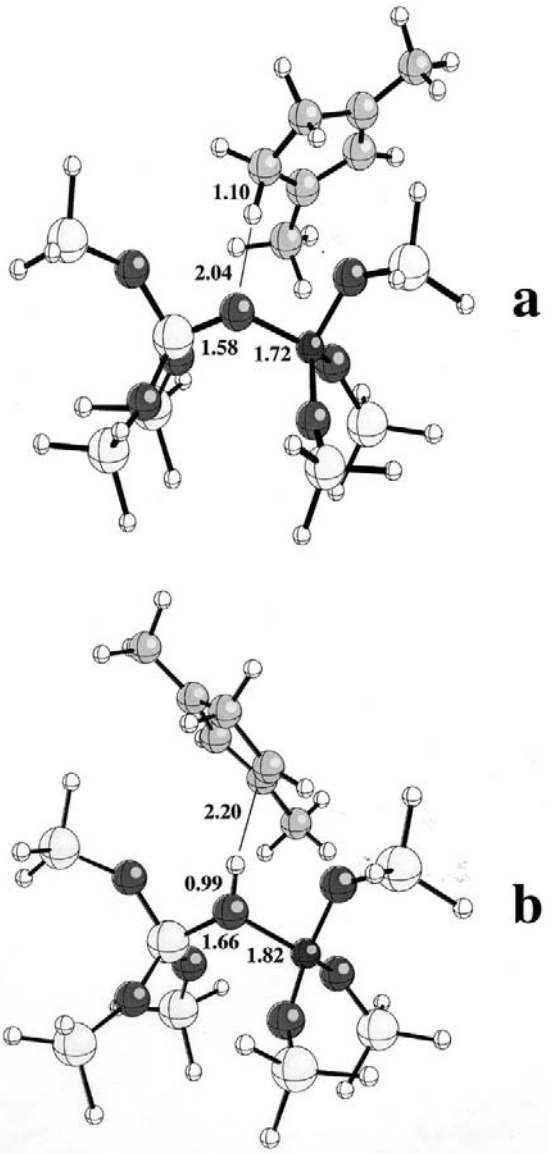


**Fig. 7** (a) DFT (B3LYP/6-311G**) optimized geometry of the 1,3-dimethylcyclopentadienyl cation coordinated to the zeolite anion (ion-pair structure). (b) DFT (B3LYP/6-311G**) optimized geometry of the $\pi$ complex formed by transferring the proton back to the zeolite acid site model. These are two stable states on the potential energy surface for this system.

increases, but the machine time required to complete a calculation can scale severely with the number of basis sets. Basis sets are typically named in a systematic way, but the nomenclature schemes vary for different schemes as with sets of trade names.

The restricted Hartree-Fock method is one electronic structural theory that carries out numerical solutions to the Schrodinger equation with neglect of electron correlation. Correlation effects can be introduced using a number of methods, including perturbation

theory. MP2 calculations include pair-wise electron correlation, but at the cost of greatly increasing the length of the calculation.

As an alternative to numerical solution of the Schrodinger equation, some properties of a molecular system can be computed as a functional (i.e., a function of a function) of electron density. Density functional theory (DFT) methods have matured to the point where energies (and therefore structures) can be computed with accuracies approaching those of MP2 methods, but at a fraction of the cost. Several functionals are commonly used in chemistry; those that include the gradient of electron density are more accurate than "local" functionals. Functionals are sometimes named after the inventors by

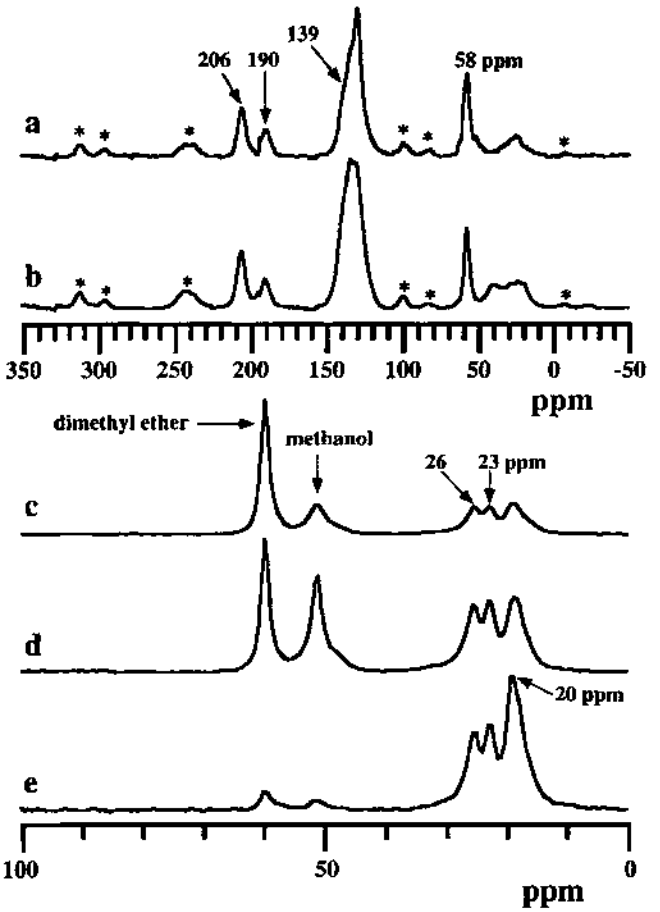


**Fig. 8** Selected 75.4-MHz $^{13}C$ MAS spectra of a pentamethylbenzenium cation (206, 190, 139, 58, and incompletely resolved signals between 23 and 26 ppm) on zeolite HZSM-5. Signals near 20 ppm are due to the methyl carbons of neutral aromatic compounds, e.g., toluene and xylenes. Benzene or toluene and methanol were injected into the flow reactor as a pulse and allowed to react for 4 s at 300°C before quench: (a) 0.5 eq of benzene-$^{13}C_6$ and 3 eq of methanol-$^{12}C$; (b) 0.5 eq of toluene-ring-$^{13}C_6$ and 2.5 eq of methanol-$^{12}C$; (c) 0.5 eq of benzene and 3 eq of methanol-$^{13}C$; (d) 0.5 eq of toluene and 2.5 eq of methanol-$^{13}C$; and (e) 0.5 eq of toluene-$^{13}C_6$ (ring) and 2.5 eq of methanol-$^{12}C$. 0.1 eq on this catalyst corresponds to 0.58 mmol reactant/g of zeolite. An asterisk denotes a spinning sideband.

combining the first letters of last names. Numbers added to the functional name may relate to a technical detail or simple chronology. The B3LYP functional (48), developed by Becke based on previous work by Lee, Yang, and Parr (49), uses three parameters to mix in some of the exact quantum mechanical exchange. It is customary to specify first the theory and then the basis sets, with a slash separating the two; the structures in Fig. 7 were optimized using DFT at the B3LYP/6-311G** level.

Further discussion of basis sets and other details of computational chemistry is clearly outside the scope of this chapter, and the reader is directed to references that introduce the topic at a textbook level (50–52). The most important point for the reader is that theory will make huge contributions to the elucidation of organic reactions in zeolites, and a student of zeolite chemistry will absolutely need to have some degree of appreciation of its strengths and weakness, as well as fluency in its vocabulary.

We end this section with one more example that has a very direct bearing on the remainder of the chapter. In situ NMR experiments using a quench reactor detected a very unusual organic species in HZSM-5 following the reaction of benzene with an excess of

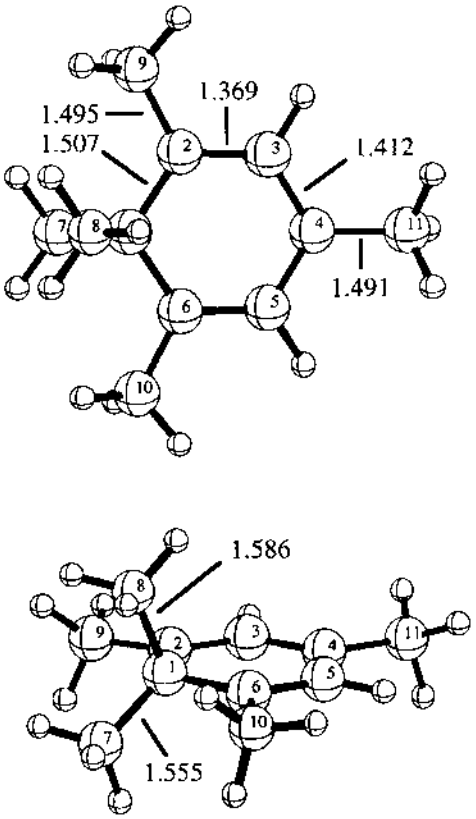


**Fig. 9** B3LYP/6-311G** geometry of a pentamethylbenzenium cation optimized in *Cs* symmetry. Selected internal coordinates are shown (in Å). The angle C-7 to C-1 to C-4 is 113.9°, C-8 to C-1 to C-4 is 137.4°, and C-8 to C-1 to C-7 is 108.7°. Theoretical $^{13}C$ isotropic chemical shifts are calculated at GIAO-MP2/tzp/dz and referenced to TMS at the same level of theory (absolute shielding 198.8 ppm): C-1, 65 ppm; C-2 and C-6, 209 ppm; C-3 and C-5, 139 ppm; C-4, 191 ppm; C-7, 23 ppm; C-8, 35 ppm; C-9 and C-10, 28 ppm; C-11, 29 ppm.

methanol (Fig. 8) (53). It had very distinctive $^{13}C$ chemical shifts including 206, 190, and 58 ppm. These signals were observed only when the $^{13}C$ was introduced in the benzene, so it was reasonable to assign these to carbons on the ring of some product. Benzene has a $^{13}C$ chemical shift of 129 ppm; the shifts at 206 and 190 ppm are suggestive of a carbenium ion, and that at 58 ppm an $sp^3$-hybridized carbon. Various lines of evidence led us to propose that the NMR spectrum was that of a pentamethylbenzenium cation with two of the methyl groups on the same ring carbon. We optimized the structure of this cation at B3LYP/6-311G**, and this structure is shown in Fig. 9. We then used other computational methods to calculate the chemical shifts of this structure at GIAO-MP2, a particularly reliable method for $^{13}C$ shifts (54). The theoretical $^{13}C$ shifts obtained were in excellent agreement with the in situ NMR experiment, and the formation of this benzenium ion in the zeolite was strongly verified. Using this same combination of experiment and theory, we recently established that the heptamethylbenzenium cation forms in the large-pore zeolite HBEA from benzene and methanol.

## IV. THE HYDROCARBON POOL MECHANISM

### A. Evidence for the Availability and Reactivity of Intermediates

In situ NMR has provided much of the direct experimental evidence, pro and con, for the existence of various species in zeolites. For example, both the framework-bound methoxonium species (27,28) and the trimethyloxonium ion (25,55) have clearly been detected under suitable conditions. An extensive set of in situ NMR experiments was carried out to see whether or not oxonium ions and related cations influence methanol conversion catalysis. For example, the trimethylsulfonium cation is more stable than the trimethyloxonium ion, and it forms at appreciable steady-state concentrations if a small amount of dimethylsulfide is introduced into HZSM-5 with methanol. However, it does not accelerate the rate of hydrocarbon synthesis. Oxonium-ylides (Scheme 2) have never been directly observed in zeolites by any experimental method. Of course, reactive intermediates are frequently present at very small steady-state concentrations, and they may escape detection by NMR or any form of spectroscopy. Also, they may form only under very special conditions, and in situ spectroscopy may fail to duplicate these conditions. Oxonium cations clearly form in acidic zeolites, and on that basis alone they are plausible intermediates in methanol to hydrocarbon catalysis; however, when put to the test they fail. Onium ions do not catalyze the formation of hydrocarbons.

One of the great misconceptions of zeolite chemistry is that they are solid superacids, i.e., acids far stronger that sulfuric acid. If zeolites are superacids, then it is reasonable to imagine that the full bestiary of exotic organic cations observed or proposed in magic acid solutions also exist in acidic zeolite, especially three-coordinate carbenium ions and five-coordinate carbonium ions. Up until a few years ago it was common to explain not only methanol conversion catalysis but also most other organic transformations on acid zeolites using very unstable cation intermediates. For example, it was assumed that propene formed the isopropylcarbenium ion at high concentrations in zeolites and that benzene was completely protonated to form $C_6H_7^+$. NMR experiments showed that neither prediction was true. The $^{13}C$ spectrum of benzene in various zeolites shows no protonation shift, and H/D exchange between benzene-$d_6$ and zeolite acid sites proceeds very slowly at room temperature (56). DFT calculations show that the mechanism of this H/D exchange is a concerted reaction without a benzenium intermediate. Other in situ NMR experiments following the fate of $^{13}C$ labels on zeolites show that the isopropyl cation is not even a transient intermediate during the reactions of propene, as equilibration with protonated

cyclopropane would scramble a $^{13}C$ label initially in one position into all three positions (57). Other NMR experiments using Hammett bases (58) or other acidity probes (59) rank the strength of zeolites well below that of sulfuric acid.

Thus, direct experiments show that most simple carbocations are not so easily formed in zeolites, and this observation challenges not only some of the direct mechanisms for methanol conversion catalysis but also long-accepted views of other reactions including hydrocarbon cracking. However, spectroscopy has confirmed the presence of other, far more stable carbenium ions on acidic zeolites. Figure 6 showed the formation of the 1,3-dimethylcyclopentenyl cation from the reactions of ethylene on HZSM-5. A variety of cyclopentenyl cations with diverse substitution patterns have been characterized on various solid acids. For example, the reactions of acetone on HSAPO-34 lead to a variety of products, including the heptamethylcyclopentenyl cation, and this appears to be an intermediate in the formation of methylbenzenes on that catalyst (60). We also saw that another type of cyclic, resonance-stabilized carbenium ion, methylbenzenium cation, forms in zeolites by extensive methylation of benzene with methanol. A third class of cyclic carbenium ion, indanyl cation, was identified in a study of the oligomerization and cracking of styrene and α–methylstyrene on the large-pore zeolite HY (61). Scheme 10 shows that the cyclic dimer of styrene (formed below room temperature) cracks to eliminate benzene, forming the methylindanyl cation. At higher temperature this cation loses hydrogen and yields naphthalene.

Astonishingly, these three types of cyclic, resonance-stabilized tertiary carbenium ions are the simplest carbocations that have been shown to persist indefinitely at room temperature on acidic zeolites. (Another large carbenium ion, the trityl cation, can be formed by halide abstraction) (62). In contrast, attempts to form many other simpler carbenium ions in zeolites were unsuccessful. It proved possible to rationalize a wide range of observations by considering the acid strengths of various carbenium ions.

Many carbenium ions are at least formally derived from a "parent" olefin or aromatic by a protonation step. For example, the isopropyl cation $C_3H_7^+$ can be formed by protonation of propene, $C_3H_6$. For an acid of fixed strength, the relative ease of protonating a given hydrocarbon should depend on its relative base strength. For example, the gas phase proton affinity of propene is 179.6 kcal/mol, and that of the more basic hydrocarbon styrene is 193.8 kcal/mol (63). Neither is protonated to form a persistent carbenium ion in zeolites; this requires more basic hydrocarbons. Figure 10 shows theoretical structures of the three parent olefins that are protonated to form the methylindanyl, dimethylcyclopentenyl, and pentamethylbenzenium cations described previously. Note the exocylic double bond on the triene that is protonated to (formally) yield the

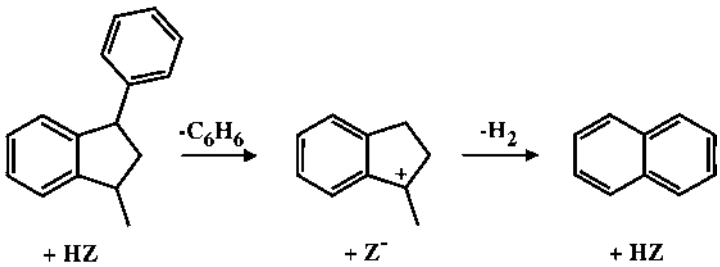


**Scheme 10** The dimer of styrene cracks on zeolite HY to form the methylindanyl carbenium ion, and this loses hydrogen to form naphthalene.

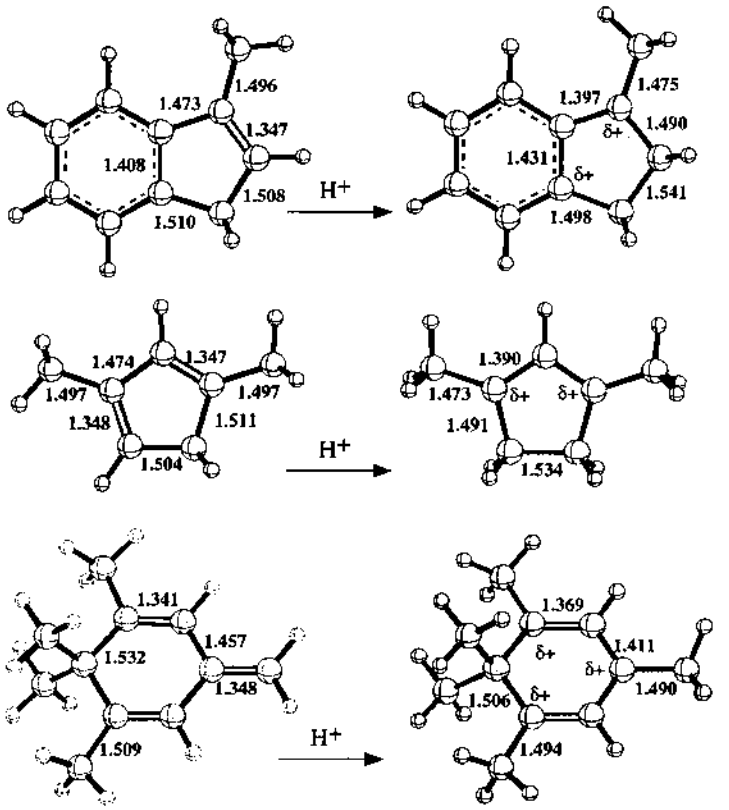


**Fig. 10** B3LYP/TZVP-optimized geometries of olefins and corresponding carbenium ions. Selected bond distances (Å) are indicated. Distances related by symmetry are not shown. Bond orders are graphically shown only for the parent olefins, for which the assignment is unambiguous. The positively charged carbons (determined by a Mulliken population analysis) of the carbenium ions are labeled.

pentamethylbenzenium cation. The three neutral olefins in Fig. 10 are real compounds that have been synthesized, but their gas phase thermochemical properties have not been studied. Therefore, we used theoretical methods to calculate their proton affinities. Table 1 reports our calculated values and compares them to experiment where available (64). We optimized the geometries of the neutrals and cations using DFT (B3LYP) and then calculated single-point energies on these structures using very demanding MP4 calculations. Energies are converted to enthalpies using other results from theory, and the proton affinity (PA) values in the Table are the $-\Delta H$ values for the protonation reactions. The accuracy of the PA values is quite high for the methods we use; in this case, experiment and theory typically agree within 2 kcal/mol. Table 1 shows that the hydrocarbons that are formally protonated to form the three types of persistent cyclic carbenium ions are exceptionally strong bases, with PA values between 209.8 and 227.4 kcal/mol. To understand how basic this range really is, consider the fact that pyridine has a PA of 222.0 kcal/mol! The sum total of evidence places the minimal basicity for quantitative protonation of a hydrocarbon in zeolite HZSM-5 in the vicinity of 207–209 kcal/mol. Thus, it is not surprising that benzene and propene, fantastically weaker bases, with PA values 30 kcal/

**Table 1** Proton Affinities of Various Hydrocarbons (kcal/mol)

| Hydrocarbon | Experimental | Theory |
|---|---|---|
| Benzene | 179.3 | 178.3 |
| Propene | 179.6 | 177.4 |
| Cyclopentene | 183.0 | 181.3 |
| Allene | 185.3 | 185.0 |
| Toluene | 187.4 | 186.0 |
| 2-Methylpropene | 191.7 | 192.5 |
| *m*-Xylene | 193.8 | |
| Styrene | 200.3 | |
| Hexamethylbenzene | 205.7 | |
| α-Methylstyrene | 206.4 | |
| 1-Methylindene | | 209.8 |
| 1,3-Dimethylcyclopentadiene | | 215.6 |
| 1,5,6,6-Tetramethyl-3-methylenecylclohexa-1,3-diene | | 227.4 |
| Pyridine | 222.0 | 219.1 |

mol lower, are not protonated at all in the zeolite. Transient protonation of hydrocarbons with basicities slightly below 207 kcal/mol cannot be ruled out.

In conclusion, the evidence is against simple carbenium ions as intermediates in methanol conversion catalysis, but resonance-stabilized cyclic carbenium ions do exist in zeolites and may suggest alternative possibilities for carbenium ion chemistry in zeolites. The chemistry of these cations in zeolites is being revealed through a combination of NMR and theoretical methods. For example, samples of HZSM-5 catalyst containing small amounts of the 1,3-dimethylcyclopentenyl cation are active for methanol conversion catalysis under conditions in which otherwise identical catalysts with no organic adsorbates (other than methanol and DME) show no activity.

### B. Failure of All Direct Mechanisms

Hydrocarbon pool mechanisms are indirect routes from methanol and DME to hydrocarbon products. Some large hydrocarbon pool compound must be methylated repeatedly by methanol/DME, and this even larger intermediate then splits off an olefin product and regenerates something very similar or identical to the original pool compound to complete a catalytic cycle. All other mechanisms are direct routes in that two to four carbons from methanol/DME come together to form ethylene or sometimes another small olefin as the first stable hydrocarbon on the reaction pathway.

In considering direct vs. indirect routes for methanol conversion catalysis, there are three general possibilities: (a) All hydrocarbon products are formed by one of the direct routes, and the indirect route (hydrocarbon pool) contributes nothing. Homologation reactions (e.g., ethylene methylated to propene) may still occur, but this reaction is distinct from the synthesis of the "first" olefins. (b) One of the direct routes operates, but only a fraction of the hydrocarbon products are directly obtained. The olefin products from the direct route form secondary products (e.g., methylbenzenes) that once formed serve as "cocatalysts" as proposed by Mole and coworkers. If the rate of the direct route is low enough it may present itself as a kinetic induction period prior to the onset of indirect conversion as the hydrocarbon pool is formed and takes over to afford a "working

catalyst." (c) No direct route operates on typical methanol conversion catalysts at typical temperatures. All catalysis is due to the indirect (hydrocarbon pool) route. Activity and selectivity depend on the concentrations and identities of various hydrocarbon pool molecules in the catalyst bed.

It has been known for some time that methanol conversion on HZSM-5 exhibits a kinetic induction period; this phenomenon has been rationalized in the context of various direct mechanisms, but it is naturally accounted for by the hydrocarbon pool mechanism. It has been shown that the deliberate introduction of olefins or higher alcohols (olefin precursors) eliminated the induction period for a pulse of methanol delivered much later. These results could be consistent with the second possibility discussed above in that direct introduction of olefins establishes a working catalyst and eliminates the wait for organic cocatalysts to form through an inefficient direct route.

We recently realized that if the rate of the direct route from methanol to olefins was very low, its measurement would require extremely careful experimental conditions to eliminate all sources of organic impurities, especially olefins, aromatics, alcohols, aldehydes, and ketones. Even analytical reagent methanol can contain tens of ppm of ethanol and ppm levels of isopropanol and acetone. We purified our best methanol using several distillation steps, including one pass through a 4-foot fractionating column, and obtained methanol with only about 2 ppm ethanol and about 11 ppm total organic impurities (by GC). We added two hydrocarbon traps between the He cylinder and a benchtop flow reactor to prevent the introduction and accumulation of organic impurities from carrier gas during activation and testing. Finally, we discovered that very small amounts of phenanthrene and other aromatic hydrocarbons are produced on the catalyst during pyrolysis of the organic templating agent used during zeolite synthesis. A modified calcination procedure was developed to reduce these impurities.

In short, we found that the first-pulse rates of volatile hydrocarbon formation on both HZSM-5 and HSAPO-34 could be made arbitrarily low as we increasingly purified our reagents to remove hydrocarbon pool precursors. The GC traces in Fig. 11 show an example for the case of HSAPO-34 (65). On this catalyst, the first pulse of methanol produced a total yield of olefins of only 0.0026%. As subsequent pulses reached the same catalyst bed its activity gradually increased due to the accumulation of impurities, but it was still very far below the 100% conversion seen with a working catalyst under otherwise similar conditions. The topmost GC trace in Fig. 11 shows the activity of the catalyst bed after a total of 250 μl of purified methanol (equivalent to 20 pulses). Even here conversion was still below 100%.

We thus reached the counter-intuitive finding that methanol/DME is not noticeably reactive on HZSM-5 and HSAPO-34 under the conditions used *in the absence of organic impurities that provide a primordial hydrocarbon pool*. Thus, we ruled out all of the direct mechanisms, at least for the most commonly used catalysts and typical reaction conditions. Only the indirect route (hydrocarbon pool) accounts for methanol conversion catalysis.

### C. Methylbenzene-Based Pool on HSAPO-34

Earlier we showed that dimethylcyclopentenyl cations readily form on HZSM-5 and accelerate the rate of methanol conversion. These cations are intermediates in the formation of toluene (20), and Mole much earlier showed that aromatic hydrocarbon to be a cocatalyst for methanol conversion on HZSM-5 (37,38). HSAPO-34 and closely related catalysts are likely to be commercialized as MTO catalysts. Aromatics cannot

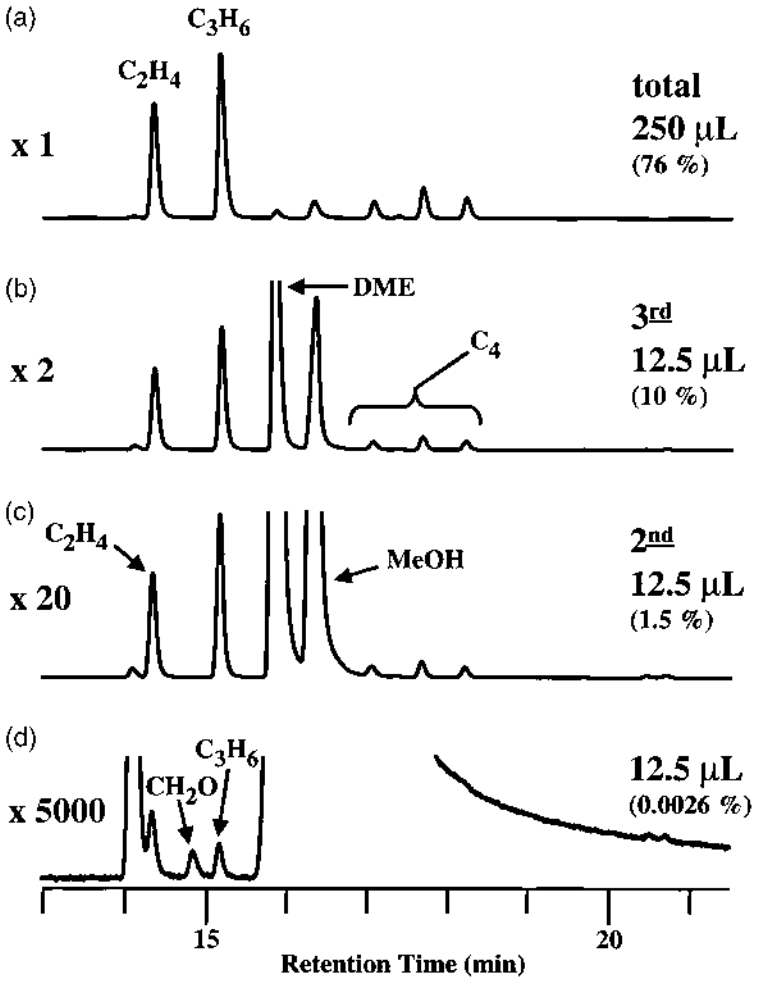


**Fig. 11** GC (flame ionization detector) analyses of the product streams sampled 2.4 s after pulsing 12.5 μl methanol onto 300-mg beds of HSAPO-34 with purified He flowing at 10 $cm^3s^{-1}$. (a)–(d) are from a single bed of rigorously calcined HSAPO-34 following a series of pulses of fractionally distilled methanol delivered at 30-min intervals. (a) Following the first pulse, the total yield of volatile hydrocarbons was about 0.0026% (26 ppm). (b) Following a second, identical methanol pulse the yield of volatile hydrocarbon products greatly increased to 1.5%. (c) Following a third, identical methanol pulse the hydrocarbon yield further increased to 10% as a result of the growing hydrocarbon pool. (d) This catalyst bed was reacted with an additional 200 μl of methanol to create a larger hydrocarbon pool. Thirty minutes later 12.5 μl of methanol was pulsed, and the product stream showed nearly complete conversion.

escape from the cages of HSAPO-34, and the weaker apparent acid strength of this catalyst compared to HZSM-5 minimizes secondary reactions of the primary products, ethylene and propene. Figure 11 strongly suggests that a hydrocarbon pool operates on HSAPO-34, but it does not suggest the identity of the hydrocarbon pool molecules. The GC traces in Fig. 12 provide a related line of evidence for a hydrocarbon pool mechanism (21). When a first pulse of normal analytical grade methanol was applied

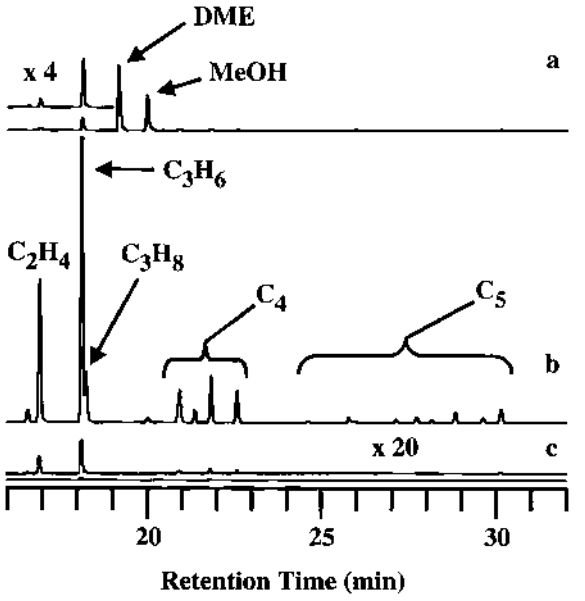


**Fig. 12** GC (flame ionization) analyses of the gases exiting the HSAPO-34 catalyst bed. Identical 20 μl methanol pulses were applied at 0 s and at 360 s: (a) 4 s after a first pulse the total conversion of methanol and dimethyl ether (DME) to hydrocarbons was only about 14%. (b) 364 s after the first pulse and 4 s after the second pulse, the conversion was essentially 100%. (c) This control experiment shows that only traces of products exit the reactor 358 s after the first methanol pulse; hence, the products observed at 364 s reflect conversion of the second methanol pulse.

to a fresh bed of HSAPO-34, the catalyst was not very active—conversion was only 14%. After waiting 360 s, a second identical pulse of methanol was introduced, and this time the catalyst achieved nearly 100% conversion. The control experiment in Fig. 12c shows only traces of volatile products evolving from the catalyst 358 s after the first pulse. Thus, homologation of olefins from the first pulse does not account for the conversion of second-pulse methanol. As demonstrated by Kolboe, when similar experiments are performed using a first pulse of methanol-$^{13}$C and a second pulse of methanol-$^{12}$C, the olefin products captured after the second pulse contain roughly equal amounts of both labels.

A quench reactor was used to study the reaction of methanol-$^{13}$C on HSAPO-34 by $^{13}$C solid-state NMR (21). Representative NMR spectra, obtained at various times following a pulse of methanol-$^{13}$C onto a fresh catalyst bed, are shown in Fig. 13. The labeled $^{13}$C used in this experiment contained 300 ppm ethanol, which afforded a primordial hydrocarbon pool. At short reaction times the organic matter trapped on the quenched catalyst was entirely methanol (50 ppm) and framework methoxonium species (56 ppm). After 4 s, methylbenzenes were clearly evident. After 16 s the intensity of aromatic ring carbon signals (about 129 ppm) did not change, even after hours at 350°C with flowing He. This is because benzene cannot pass through the 8-ring windows connecting cages in HSAPO-34. Note that the signal for methyl groups on aromatic rings (about 20 ppm) does decrease over time, suggesting that these are lost in the production of olefins.

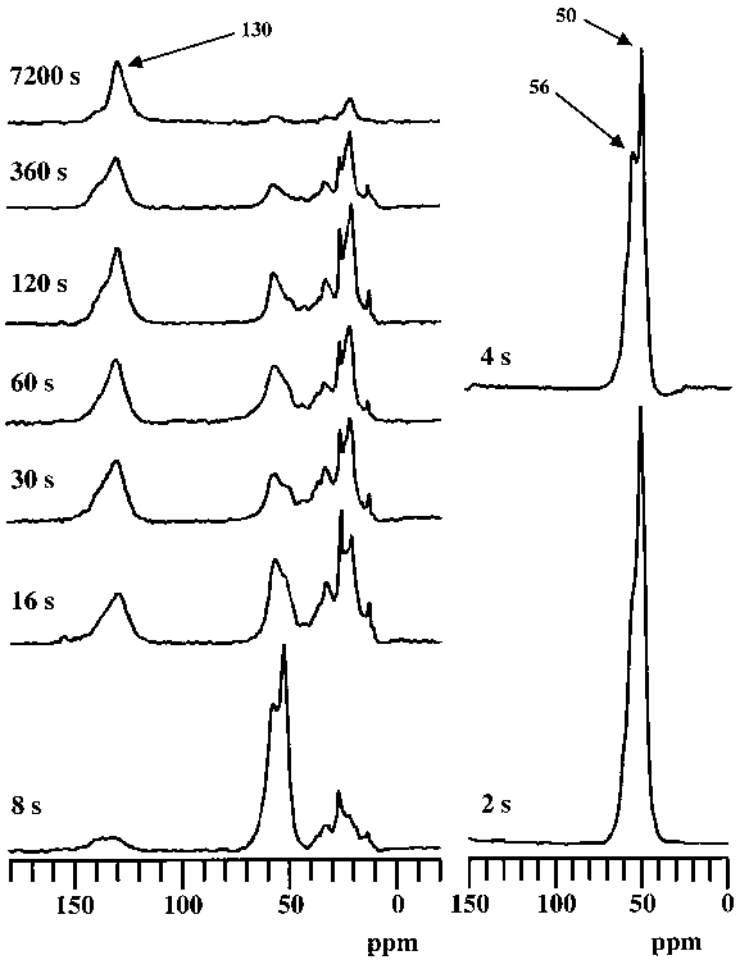


**Fig. 13** 75 MHz $^{13}C$ CP/MAS NMR spectra of samples from a pulse-quench study of methanol conversion on HSAPO-34 at 400°C. Each sample was prepared by injecting 20 μl of methanol-$^{13}C$ onto a freshly activated catalyst bed (0.3 g) while He was flowed at 600 ml $min^{-1}$, and reaction occurred for the times shown followed by a rapid thermal quench. All spectra (4000 scans) were measured at 25°C using a 2-ms contact time.

### D. How Does the Hydrocarbon Pool Work?

All hydrocarbon pool species identified thus far are cyclic organic species that can cycle between neutral molecules and relatively stable carbenium ions on the catalyst. Methylbenzenes have been studied in the most detail, and we will consider two mechanisms proposed for the detailed conversion of methanol to olefins via methylbenzene intermediates. With a high methanol space velocity, a benzene ring in an HSAPO-34 cage or in the channel of zeolite HBEA is readily methylated to penta- or hexamethylbenzene (24). We have also shown that on HBEA a final methylation produces the heptamethylbenzenium cation as a stable species (66). On the medium-pore zeolite HZSM-5, methylation may not go beyond tetramethylbenzene and a

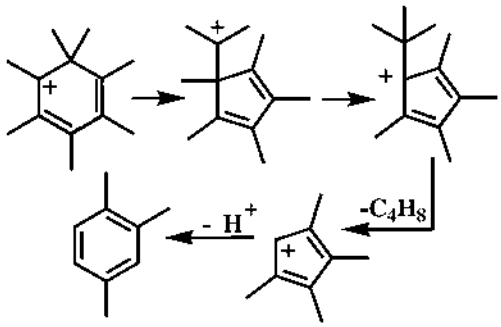


**Scheme 11** The paring reaction. Formation of butene is shown as an example.

pentamethylbenzenium ion (53), in which case the detailed steps below should be envisioned with two fewer methyl groups.

The paring reaction was proposed in 1961 (67) to account for some of the steps in the hydrocracking of hexamethylbenzene on a bifunctional catalyst. Scheme 11 is a simplified version of that mechanism showing formation of butene as an example. The original paring mechanism featured cations produced by protonation, but we favor gem-dimethyl cations such as the heptamethylbenzenium cation because their existence in zeolites is established (53,66). The essential feature of the paring mechanism is 6 ⇆ 5 ring contraction-expansion steps that extend an alkyl chain from the ring. Once an ethyl, isopropyl, or other chain is extended, it is easily lost to form the corresponding olefin. The methylbenzene loses methyl groups in the process, and several remethylation steps complete the catalytic cycle. A possible test of the paring reaction is to selectively label the ring carbons with $^{13}C$ and look for this label in the olefin products. This happens under some circumstances (but not others), and its interpretation is not conclusive. Another possible way to scramble ring and methyl carbons is ring expansion-contraction (6 ⇆ 7) through benzyl and tropylium cations. The paring mechanism probably contributes to olefin synthesis from methanol, at least under some conditions, but the evidence is stronger for a second mechanism.

The side-chain mechanism originated with Mole's explanation of the effect of added toluene (Scheme 8) (37,38). We envision deprotonation of a gem-dimethylbenzenium cation (e.g., heptamethylbenzenium) as in Scheme 12. The exocyclic olefin this produced is readily methylated under MTO reaction conditions to form first an ethyl and then an isopropyl group as depicted in Scheme 13. Either of these is eliminated to form a primary olefin product and hexamethylbenzene or some other active hydrocarbon pool molecule is regenerated. The side-chain mechanism does not predict incorporation of ring carbons into olefin products, but this could still happen through scrambling routes unrelated to olefin synthesis.

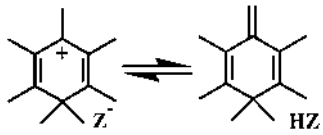


**Scheme 12** Deprotonation of the heptamethylbenzenium cation to form an exocyclic olefin.

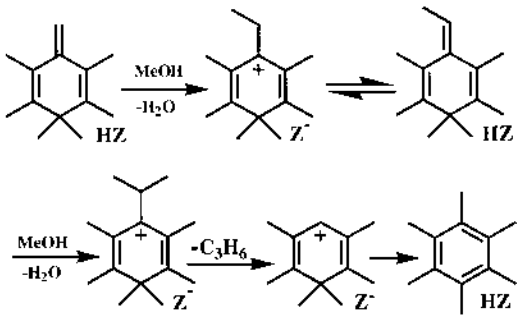


**Scheme 13** Side-chain mechanism.

One approach to the study of methylbenzene chemistry in zeolites would be to pulse them onto a catalyst, either alone or with methanol-$^{13}$C, and use GC-MS to study activity for olefin formation, product selectivity, and the fate of the carbon labels. This simple approach is not possible with small-pore HSAPO-34, and some but not all methylbenzenes can enter medium-pore HZSM-5, but large-pore HBEA readily admits hexamethylbenzene. The total ion chromatograms in Fig. 14 show the products from otherwise identical experiments in which methylbenzenes with three, four, five, or six methyl groups were pulsed onto HBEA catalyst beds at 450°C (24).

Several organic reactions are evident in the figure: More than one isomer of trimethylbenzene and tetramethylbenzene exist, and the pure isomers introduced in Fig. 14a and b equilibrated with the other possibilities. For example, all three isomers of trimethylbenzene were obtained from 1,2,4-trimethylbenzene. Second, disproportionation occurred in every case. For example, 1,2,4-trimethylbenzene also yields some xylenes and tetramethylbenzenes. Disproportionation also apparently occurred for hexamethylbenzene; note in Fig. 14d that the major products were pentamethyl- and hexamethylbenzenes. Scheme 14 shows that hexamethylbenzene disproportionation is possible if the heptamethylbenzenium cation is formed. The alternative reaction in Scheme 15 shows that hexamethylbenzene could also transfer a methyl group to the zeolite to form pentamethylbenzene and a framework methoxonium species.

Finally, the methylbenzenes eliminate light olefins, especially ethylene and propene. Olefin yield increased with the number of methyl groups on the ring, but with hexamethylbenzene the yield was only about 2%. The olefin yield from pure methylbenzenes could be increased moderately using higher temperature or acid site density. Secondary reactions of the olefinic products, especially formation of isobutane, are also evident in Fig. 14c and d. Olefin disproportionation results in formation of alkanes and aromatics. These reactions increase with acid strength and site density.

Figure 15 explores the effect or coinjecting methylbenzenes and methanol-$^{13}$C (24). Figure 15a repeats hexamethylbenzene alone for comparison. Figure 15b shows that a vastly higher olefin yield is obtained from a 5:1 mixture of methanol-$^{13}$C and toluene; a similar result was also obtained with 3:1 methanol-$^{13}$C to trimethylbenzene. The control experiment in Fig. 15d is 5:1 water to hexamethylbenzene; this experiment would entail the same composition as 5:1 methanol to toluene if ring methylation went to completion before any other reaction, clearly this was not the case as 15d has the same low olefin yield as hexamethylbenzene alone.

Table 2 reports the $^{13}$C label distributions in ethylene and propene from the experiments in Fig. 15b and c as well as closely related experiments using zeolites with

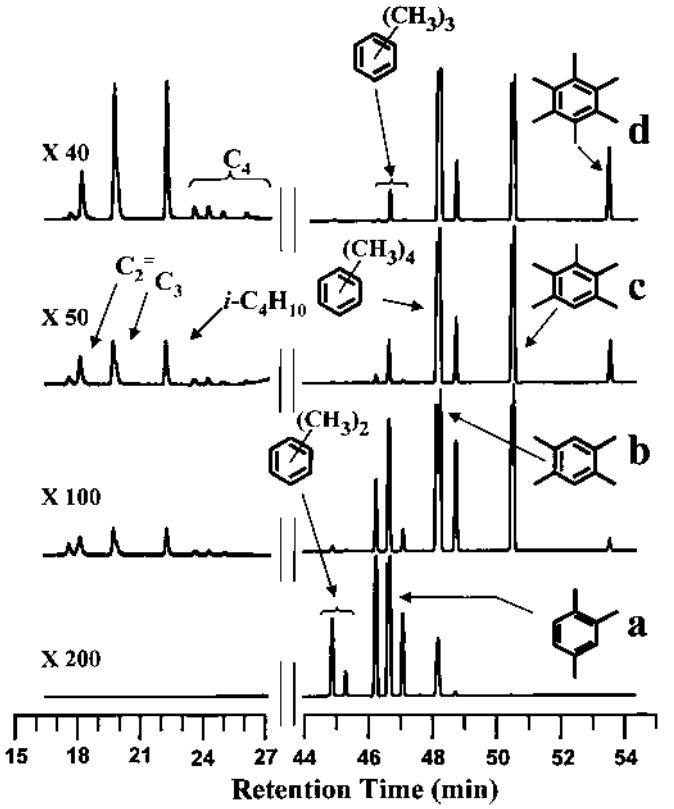


**Fig. 14** GC-MS total ion chromatograms from analyses of the volatile products exiting a catalytic reactor (300 mg zeolite HBEA, $SiO_2/Al_2O_3 = 75$, 450°C) sampled 1.5 s following pulsed introduction of 0.123 mmol of various pure methylbenzene compounds. This loading corresponds to one molecule per acid site in the catalyst bed. Several of the more intense peaks in this and similar figures show structure due to overloading. The short retention time regions (olefins and light alkanes) are amplified as necessary for visualization of these products. (a) 1, 2, 4-Trimethylbenzene isomerizes and disproportionates but produces no detectable olefins on HBEA. (b) Durene (1,2,4,5-tetramethylbenzene) also isomerizes and disproportionates, and it eliminates 0.2% olefins with the highest ethylene selectivity in the figure. (c) Pentamethylbenzene disproportionates and yields about 1% olefins and alkanes. (d) HMB eliminates a relatively higher yield of olefins, 2%, with the highest propene selectivity in the figure. The large amounts of pentamethylbenzene and tetramethylbenzenes cannot be accounted for olefin elimination alone.

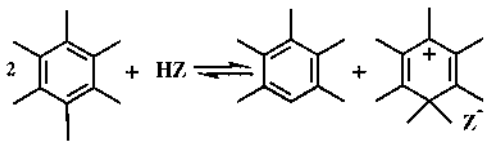


**Scheme 14** Disproportionation of HMB on zeolite HBEA.

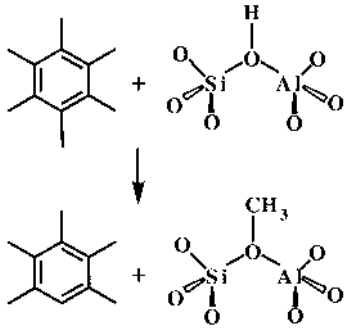

**Scheme 15** Methylation of zeolite NBEA by HMB.

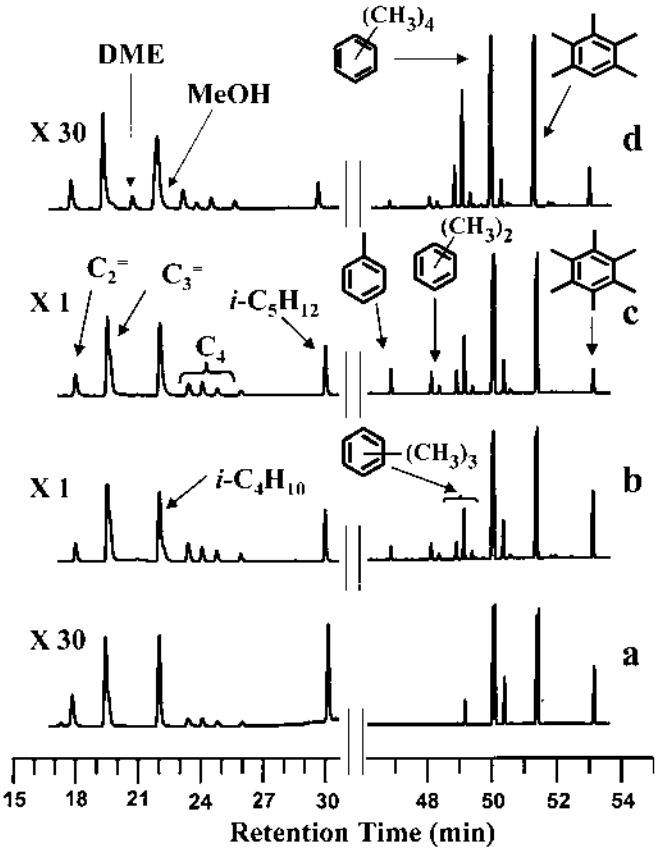


**Fig. 15** GC-MS total ion chromatograms from experiments probing the reactions of methylbenzenes with methanol-$^{13}$C. All experiments shown were carried out at 450°C using HBEA with $SiO_2/Al_2O_3$ = 75 and gas sampling at 1.5 s. (a) HMB alone as a control. (b) Methanol-$^{13}$C and toluene 5:1 (molmol). (c) Methanol-$^{13}$C and 1, 2, 4-trimethylbenzene 3:1 (molmol). (d) Control experiment using water and HMB 5:1 (molmol). The solutions of methylbenzenes and methanol yielded far more olefins than the controls. Note that the overall stoichiometries of experiments (b) and (d) are similar and would be identical if the conversion of toluene methanol to HMB and water went to completion before any other step.

**Table 2** Carbon Label Distribution in Ethylene and Propene for Various Reactions

| System | $\%^{13}C$ in starting material[a] | $\%^{13}C_3$ in starting material[b] | Ethylene | | | | Propene[c] | | | | |
|---|---|---|---|---|---|---|---|---|---|---|---|
| | | | Total $^{13}C$ in ethylene (%) | $^{13}C_0$ (%) | $^{13}C_1$ (%) | $^{13}C_2$ (%) | Total $^{13}C$ in propene (%) | $^{13}C_0$ (%) | $^{13}C_1$ (%) | $^{13}C_2$ (%) | $^{13}C_3$ (%) |
| $^{13}C$-$CH_3OH$ + Toluene (5:1) on HBEA (75) | 83.3 | 83.3 | 83.8 | 6.1 | 20.2 | 73.7 | 87.2 | 0.0 | 5.0 | 28.7 | 66.3 |
| $^{13}C$-$CH_3OH$ + 1,2,4-trimethylbenzene (3:1) on HBEA (75) | 50.0 | 50.0 | 62.2 | 17.6 | 40.7 | 41.8 | 75.1 | 1.0 | 14.5 | 42.9 | 41.6 |
| $^{13}C$-$CH_3OH$ + 1,2,4-trimethylbenzene (3:1) on HBEA (150) | 50.0 | 50.0 | 47.9 | 33.8 | 36.6 | 29.6 | 61.8 | 13.0 | 21.7 | 31.7 | 33.5 |
| $^{13}C$-$CH_3OH$ + 1,2,4-trimethylbenzene (3:1) on HBEA (300) | 50.0 | 50.0 | 50.2 | 30.5 | 38.6 | 30.9 | 72.4 | 2.2 | 17.9 | 39.0 | 40.9 |
| $^{13}C$-$CH_3OH$ + hexamethylbenzene (5:1) on HBEA (75) | 45.5 | 45.5 | 62.3 | 21.5 | 32.5 | 46.0 | 85.6 | 3.8 | 2.0 | 28.1 | 66.1 |

[a] Includes all carbons in both reactants.
[b] Includes only methyl groups in both reactants and not ring carbons.
[c] The yield of propene is in all cases several times that of ethylene.

lower acid site densities (higher Si/Al ratios) (24). Note that the $^{13}C$ content of the olefin products is in all cases much greater than the fraction of $^{13}C$ in all starting materials. For ethylene the $^{13}C$ content is at least as great as that in all $CH_3$ groups, and for propene the $^{13}C$ content is much greater than the starting $^{13}C$ in all methyl groups. If the paring route (67) were dominant in these experiments we would expect to see much more $^{12}C$ (from ring carbons) in the product olefins. Clearly this is not the case. The isotope distributions in Table 2 are more consistent with side-chain alkylation; in the case of propene it would appear that methanol (or dimethyl ether) contributes the final carbon. This would also happen if any ethylene produced as a primary product was homologized by methanol in a subsequent step.

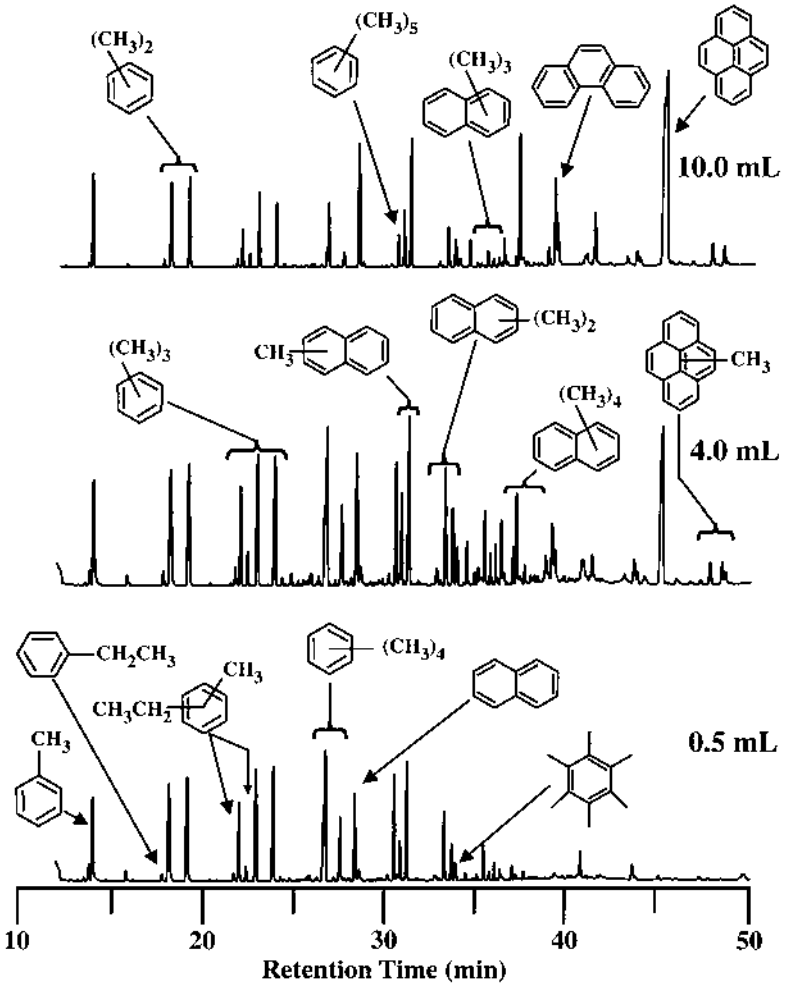


**Fig. 16** GC-MS total ion chromatograms from analyses of $CCl_4$ extracts of organics formed in HSAPO-18 catalyst beds during methanol conversion in HSAPO-18. These organics were first liberated by digesting the catalysts with 1 M HCl. While methylbenzenes are the major species present early in the lifetime of the catalyst, methylnaphthalenes are also significant after 1 or 2 ml of methanol. Phenanthrene and pyrene are prominent on the deactivated catalyst.

### E. Aging of Pool Species on HSAPO-18

Zeolite solid acid catalysts deactivate in the course of many industrial processes as a result of "coke" buildup in channels and pores. This is sometimes not so pronounced with zeolites HZSM-5 or HBEA because only the channel intersections are larger than the channels themselves. For HY (FAU) zeolites the supercages have much larger diameters than the 12-ring windows that interconnect them, and FAU-base cracking catalysts rapidly accumulate polycyclic aromatic hydrocarbons that can leave the zeolite only by combustion. The need for continuous regeneration of catalysts motivates the use of fluidized-bed reactors that constantly move catalyst between the reactor and regenerator.

"Coke" is so broad a term as to be almost useless. Coke can be amorphous carbon, high molecular weight polycyclic hydrocarbons, mixtures of aromatic hydrocarbons, methylbenzenes, branched long-chain aliphatics, or sometimes phenolic materials. There is "bad coke" and "good coke." The latter could sometimes be synonymous with a hydrocarbon pool, and these could be widely important in zeolite catalysis. A catalyst bed that is "coked up" is no longer active as a result of the accumulation of carbon-rich material that restricts mass transport through catalyst particles and/or blocks close contact with the active site.

Methanol conversion catalysis is no exception. Although HSAPO-18 requires methylbenzenes in some of its cages to be an active MTO catalyst, it requires that methanol and DME have unrestricted access to these cages, and ethylene and propene must exit the crystallite before secondary reactions occur. When it comes to the hydrocarbon pool, there can be too much of a good thing.

Figure 16 presents a series of GC-MS total ion chromatograms that profile the time evolution of the "coke" on HSAPO-18 catalyst beds (330 mg each) as a function of the total amount of methanol delivered at a space velocity of 16 $h^{-1}$. Acid digestion with 1 M HCl was used to free the organic matter for these analyses. Aluminosilicate zeolites require more demanding conditions for acid digestion, typically concentrated HF. Early in the lifetime of the catalyst bed most of the entrained molecules are methylbenzenes. Methylnaphthalenes predominate as the catalyst ages; these are also active for methanol conversion catalysis, but somewhat less so than methylbenzenes. As the catalyst deactivates it becomes congested with phenanthrene and pyrene. Aromatics larger than pyrene are not accommodated by the HSAPO-18 cages, and they are not seen in this experiment. The mechanism by which polycyclic aromatics form in zeolites is not precisely known, but it probably involves ring closure by $C_4$ chains on benzene derivatives, followed by loss of hydrogen.

## V. CONCLUSIONS

We have illustrated a number of organic reactions in acidic zeolites using methanol conversion catalysis as an example. Experimental and theoretical methods used to study reactions in zeolites were surveyed. A number of reaction mechanisms were proposed for methanol conversion catalysis, and a similar lack of consensus can be found for other reactions on solid catalysts. This chapter reviewed a number of recent studies from the authors' group that seem to elucidate the general features of the reaction mechanism and suggest more specific questions for ongoing investigations. The group of Kolboe and coworkers has come to similar conclusions regarding the nature and function of the hydrocarbon pool mechanism in methanol conversion catalysis, but not all groups will immediately agree with the picture painted here. There is an old saying in chemistry that mechanisms can never be proven, only disproven. But mechanisms can be increasingly

verified by an accumulation of experimental and theoretical evidence, and that seems to be happening here. One very promising sign that the hydrocarbon pool mechanism is valid is that it keeps generating new and productive lines of investigation, whereas some of the other mechanisms were less useful for generating new and testable hypotheses.

There is some evidence in the literature that hydrocarbon pools may govern other important reaction in zeolite catalysis. For example, small amounts of olefins have a big impact on the rates of alkane cracking reactions. Hydrocarbon pools may require a major rethinking of zeolite catalysis. What was once a simple, inorganic active site is now a much larger and far more complex hybrid organic-inorganic structure, at least for methanol conversion catalysis.

## REFERENCES


1. A Corma Chem Rev 95: 559–614, 1995.
2. A Corma Chem Rev 97: 2373–2419, 1997.
3. JM Thomas, WJ Thomas. Principles and Practice of Heterogeneous Catalysis. New York: VCH, 1996, p 515.
4. RA VanSanten, GJ Kramer. Chem Rev 95: 637–660, 1995.
5. CD Chang, AJ Silvestri. J Catal 47: 249–259, 1977.
6. CD Chang. Catal Rev Sci Eng 25: 1–118, 1983.
7. CD Chang. Catal Rev Sci Eng 26(3–4): 323, 1984.
8. FJ Keil. Micropor Mesopor Mater 29: 49–66, 1999.
9. M Stöcker. Micropor Mesopor Mater 29: 3–48, 1999.
10. S Wilson, P Barger. Micropor Mesopor Mater 29: 117–126, 1999.
11. N Tajima, T Tsuneda, F Toyama, K Hirao. J Am Chem Soc 120: 8222–8229, 1998.
12. SR Blaszkowski, RA vanSanten. J Am Chem Soc 119: 5020–5027, 1997.
13. B Arstad, S Kolboe. Catal Lett 71: 209–212, 2001.
14. B Arstad, S Kolboe J Am Chem Soc 123: 8137, 2001.
15. IM Dahl, S Kolboe. Catal Lett 20: 329, 1993.
16. IM Dahl, S Kolboe. J Catal 149: 458–464, 1994.
17. IM Dahl, S Kolboe. J Catal 161: 304–309, 1996.
18. O Mikkelsen, PO Ronning, S Kolboe. Microporous Mesoporous Mater 40: 95–113, 2000.
19. PW Goguen, T Xu, DH Barich, TW Skloss, W Song, Z Wang, JB Nicholas, JF Haw. J Am Chem Soc 120: 2651–2652, 1998.
20. JF Haw, JB Nicholas, W Song, F Deng, Z Wang, CS Heneghan. J Am Chem Soc 122: 4763–4775, 2000.
21. W Song, JF Haw, JB Nicholas, CS Heneghan. J Am Chem Soc 122: 10726–10727, 2000.
22. W Song, H Fu, JF Haw. J Am Chem Soc 123: 4749–4754, 2001.
23. W Song, H Fu, JF Haw. J Phys Chem.B 105: 12839–12843, 2001.
24. A Sassi, W Song, MA Wildman, HJ Ahn, P Prasad, JB Nicholas, JF Haw. J Phys Chem.B 106: 2294–2303, 2002.
25. EJ Munson, JF Haw. J Am Chem Soc 113: 6303–6305, 1991.
26. EJ Munson, AA Khier, ND Lazo, JF Haw. J Phys Chem 96: 7740–7746, 1992.
27. DK Murray, JW Chang, JF Haw. J Am Chem Soc 115: 4732–4741, 1993.
28. DK Murray, T Howard, PW Goguen, TR Krawietz, JF Haw. J Am Chem Soc 116: 6354–6360, 1994.
29. JP van den Berg, JP Wolthuizen, JHC van Hooff. In: Proceedings 5th International Zeolite Conference (Naples) (L. V. Rees, ed.). London, Heyden 1980, pp 649–660.
30. GA Olah, H Doggweiler, JD Felberg, S Froglich, MJ Grdina, R Karpleles, T Keumi, S Inaba, WM Ip, K Lammertsma, G Salem, DC Tabor. J Am Chem Soc 106: 2143–2149, 1984.
31. GJ Hutchings, F Gottschalk, MV Michéle, R Hunter. J Chem Soc Faraday Trans I 83: 571–583, 1987.

32. D Kagi. J Catal 69: 242–243, 1981.
33. EA Swabb, BC Gates. Ind Eng Chem Fund 11: 540–545, 1972.
34. CD Chang. J Catal 69: 244–245, 1981.
35. JKA Clarke, R Darry, BF Hegarty, E O'Donoghue, V Amir-Ebrahimi, JJ Rooney. J Chem Soc Chem Commun 425–426, 1986.
36. CD Chang, SD Hellring, JA Pearson. J Catal 115: 282–285, 1989.
37. T Mole, G Bett, D Seddon. J Catal 84: 435–445, 1983.
38. T Mole, JA Whiteside, D Seddon. J Catal 82: 261–266, 1983.
39. YS Xiong, PG Rodewald, CD Chang. J Am Chem Soc 117: 9427–9431, 1995.
40. JF Haw, ed. In Situ Spectroscopic Methods in Catalysis. New York: Wiley, 2002.
41. T Xu, JF Haw. Topics Catal 4: 109–118, 1997.
42. JF Haw, T Xu. Adv Catal 42: 115–180, 1998.
43. JF Haw. In: In Situ Spectroscopic Methods in Catalysis (J. F. Haw, ed.). New York: Wiley, 2002.
44. JF Haw, PW Goguen, T Xu, TW Skloss, W Song, Z Wang. Angew Chem 37: 948–949, 1998.
45. RF Howe. In: In Situ Spectroscopic Methods in Catalysis (J. F. Haw, ed.). New York: Wiley, 2002.
46. PC Stair. In: In Situ Spectroscopic Methods in Catalysis (J. F. Haw, ed.). New York: Wiley, 2002.
47. MJ Frisch, GW Trucks, HB Schlegel, GE Scuseria, MA Robb, et al. Gaussian 98, Revision A.4. Pittsburgh: Gaussian, Inc., 1998.
48. AD Becke. J Chem Phys 98: 5648, 1993.
49. S Lee, W Yang, RG Parr. Phys Rev B 37: 785, 1988.
50. PW Atkins, RS Friedman. Molecular Quantum Mechanics, 3rd ed. Oxford: Oxford Universtiy Press, 1997, pp 276–319.
51. JB Foresman, A Frisch. Exploring Chemistry with Electronic Structure Methods, 2nd ed. Pittsburgh: Gaussian, Inc., 1996.
52. WJ Hehre, L Radom, PvR Schleyer, JA Pople. Ab Initio Molecular Orbital Theory. New York: Wiley 1986.
53. J Gauss. Chem Phys Lett 191: 614–620, 1992.
54. T Xu, DH Barich, PW Goguen, W Song, Z Wang, JB Nicholas, JF Haw. J Am Chem Soc 120: 4025–4026, 1998.
55. EJ Munson, AA Kheir, JF Haw. J Phys Chem 97: 7321–7327, 1993.
56. LW Beck, T Xu, JB Nicholas, JF Haw. J Am Chem Soc 117: 11594–11595, 1995.
57. JF Haw, BR Richardson, IS Oshiro, NL Lazo, JA Speed. J Am Chem Soc 111: 2052–2058, 1989.
58. JB Nicholas, JF Haw, LW Beck, TR Krawietz, DB Ferguson. J Am Chem Soc 117: 12350–12351, 1995.
59. T Xu, EJ Munson, JF Haw. J Am Chem Soc 116: 1962–1972, 1994.
60. W Song, JB Nicholas, JF Haw. J Phys Chem B 105(19): 4317–4323, 2001.
61. T Xu, JF Haw. J Am Chem Soc 116: 10188–10195, 1994.
62. T Tao, GE Maciel. J Am Chem Soc 117: 12889–12890, 1995.
63. NIST Chemistry WebBook (http://webbook.nist.gov/chemistry/).
64. JB Nicholas, JF Haw. J Am Chem Soc 120: 11804–11805, 1998.
65. W Song, DM Marcus, H Fu, JO Ehresmann, JF Haw. J Am Chem Soc 124: 3844–3845, 2002.
66. W Song, JB Nicholas, A Sassi, JF Haw. Catal Lett 81(1-2): 49–53, 2002.
67. RF Sullivan, CJ Egan, GE Langlois, RP Sieg. J Am Chem Soc 83: 1156–1160, 1961.